Particle and fluid simulations of low-temperature plasma discharges: benchmarks and kinetic effects

2005 J. Phys. D: Appl. Phys. 38 R283

(http://iopscience.iop.org/0022-3727/38/19/R01)

INSTITUTE OF PHYSICS PUBLISHING JOURNAL OF PHYSICS D: APPLIED PHYSICS

J. Phys. D: Appl. Phys. **38** (2005) R283–R301 doi:10.1088/0022-3727/38/19/R01

TOPICAL REVIEW

Particle and fluid simulations of low-temperature plasma discharges: benchmarks and kinetic effects

H C Kim[1], **F Iza, S S Yang, M Radmilović-Radjenović and J K Lee**[2]

Department of Electronic and Electrical Engineering, Pohang University of Science and Technology, Pohang 790-784, Korea

E-mail: jkl@postech.ac.kr

Received 1 June 2005, in final form 4 July 2005
Published 16 September 2005
Online at stacks.iop.org/JPhysD/38/R283

Abstract

Fluid, particle-in-cell and hybrid models are the numerical simulation techniques commonly used for simulating low-temperature plasma discharges. Despite the complexity of plasma systems and the challenges in describing and modelling them, well-organized simulation methods can provide physical information often difficult to obtain from experiments. Simulation results can also be used to identify research guidelines, find optimum operating conditions or propose novel designs for performance improvements. In this paper, we present an overview of the principles, strengths and limitations of the three simulation models, including a brief history and the recent status of their development. The three modelling techniques are benchmarked by comparing simulation results in different plasma systems (plasma display panels, capacitively coupled plasmas and inductively coupled plasmas) with experimentally measured data. In addition, different aspects of the electron and ion kinetics in these systems are discussed based upon simulation results.

(Some figures in this article are in colour only in the electronic version)

1. Introduction

Plasma modelling is complicated in general. It involves the solution of neutral and charged particle kinetics, radiation transport, Maxwell equations and large numbers of volume and surface reactions. Different time and spatial scales have to be resolved simultaneously and self-consistently. Incorporating all aspects of plasma in one detailed model would therefore result in an untreatable model. Despite these difficulties, plasma modelling has become a valuable tool for understanding plasma physics and has contributed to the development of improved-performance plasma reactors/devices. This has been made possible by the development of simplified models and simulation techniques and the choice of the appropriate methods to examine particular problems [1–3].

The development of these models and simulation techniques has been an ongoing process for more than five decades, with rapid growth occurring over the last decade. Particle modelling started with pioneering work in the late 1950s and early 1960s [4–7]. The early work using fluid models involved zero-dimensional (a purely plasma chemical model dealing with volume-averaged or uniform quantities) or one-dimensional simulations of capacitively coupled discharges [8–11]. Computer resources were limited and the emphasis was on validating and refining modelling techniques by studying fundamental plasma physics. The development

[1] Present address: Plasma Theory and Simulation Group, University of California–Berkeley, USA.
[2] Author to whom any correspondence should be addressed.

of comprehensive plasma models capable of simulating different plasma reactors was only envisioned at that time. Thanks to the success of this early work and the improvement in computer performance, two- and three-dimensional models with detailed chemistry were developed in the 1990s. This coincided with the emergence of inductively coupled plasmas (ICPs). Comprehensive fluid and hybrid plasma models capturing many aspects of ICP reactors were developed at that time to help in the design and optimization of new plasma processes for the semiconductor industry [12–15]. Particle simulation limited to one-dimensional models was performed mainly on parallel plate discharges and provided important contributions to the understanding of non-local effects in capacitively coupled discharges [16–18]. Bounded models and computationally-efficient techniques to incorporate statistical collisions in particle simulations were also developed in the mid-1990s [19, 20]. In more recent years, fluid, particle and hybrid models have undergone continuous refinements, and have been adopted to simulate a large number of plasma systems.

Although plasma computational modelling has experienced an unprecedented growth in recent years thanks to the availability of high-performance low-cost computers, attention needs to be paid to the actual capabilities and limitations of current simulation techniques. As shown in the examples presented in this review, different plasma systems will require different simulation techniques in order to capture the main physics of the discharge. Despite the limitations existing in any modelling approach, an educated selection of the plasma model can lead to remarkable agreement between simulation results and experimental observations. For continued growth of the numerical modelling and simulation of plasmas, the fidelity of the simulation results needs to be confirmed.

In this paper, the fluid, the particle-in-cell Monte-Carlo-collision (PIC-MCC) and the hybrid models are reviewed. These are the models commonly used in simulating low-temperature plasmas. A brief description of the three models with emphasis on their capabilities and limitations is presented in section 2. Sections 3, 4 and 5 are devoted to the fluid, the PIC-MCC and the hybrid models, respectively. In these sections, each of the models is benchmarked by comparing simulations results with experimental measurements in either a plasma display panel (PDP) cell, a capacitively coupled discharge or an inductively couple discharge. Additionally some aspects of the electron and ion kinetics in these three systems are discussed in the light of the simulation results.

2. Plasma models

Despite the unprecedented improvement in computer performance over the last four decades, incorporating all aspects of a plasma system into one generic detailed model might result in an untreatable problem. Instead, simpler models with appropriate assumptions are commonly used. As a result, no single model can be considered 'the best' as the criteria for such a selection depend on the physics to be captured. The simplified plasma models based on educated assumptions are capable of predicting and reproducing experimental results. Thanks to this success, numerical modelling of plasmas has become a valuable tool for understanding the physics involved in low-temperature discharges and optimizing plasma sources. The model used to simulate a certain plasma system, however, should be selected based on the plasma conditions that are expected to be encountered.

In this paper an overview of the fluid, the PIC-MCC and the hybrid models is presented. These are the models commonly used to simulate low-temperature plasmas. Equations and algorithms are presented but it is not within the scope of this paper to present a numerical implementation of the models. Myriad variations exist and it would be impossible to cover all of them in detail in this paper. Instead, the general strengths and limitations of each model are pointed out to help us make an educated model selection when simulating a particular plasma system.

It is worth mentioning that the fidelity of the simulation results depends not only on the assumptions intrinsic to each model, but also on the uncertainties of the input parameters. Often, simulation input parameters such as cross sections, secondary electron emission coefficients and reaction rates are known with insufficient precision. This sets an upper limit to the fidelity of the simulation results. Nevertheless, simulations still provide insights into the physics of the discharge and general trends can be identified.

2.1. *Fluid models*

2.1.1. Description. Fluid models describe the plasma based on the density, mean velocity and mean energy of the constituent species. The values of these macroscopic quantities are obtained by solving the continuity, the flux and the energy equations for each species in the plasma. These fluid equations are obtained by taking velocity moments of the Boltzmann equation [1]. Maxwell equations (or Poisson's equation in electrostatic simulations) are coupled with fluid equations to obtain self-consistent electric/magnetic fields.

When the momentum transfer collisional frequency is larger than the radio frequency (RF) driving frequency, the drift–diffusion (DD) approximation can be used instead of the flux balance equation. In the DD approximation, the inertia of charged particles is neglected so that the mean velocities respond instantaneously to the electric field. The mean particle fluxes are determined by adding a diffusion term due to spatial density gradients and a drift term for the charged particles due to the electric field [1, 8–11, 21]. For a typical RF excitation frequency of 13.56 MHz, the DD approximation for electrons is valid for argon gas pressures above ∼100 mTorr. At lower pressures and/or higher frequencies, the full flux equation should be used to incorporate electron inertia.

Equations (1)–(6) correspond to a typical set of equations solved in a fluid simulation of a low-temperature plasma when the effect of the magnetic field is negligible. The DD approximation is used for electrons (equation (2)) whereas the full flux equation is used for the more massive ions (equation (5)). Only the equations used for electrons and a single ion species are written. The set, however, can be easily extended to consider other species. Ions are typically assumed to remain at the same temperature as the neutral gas and therefore the energy balance equation is not solved for ions.

Electrons:

$$\frac{\partial n_e}{\partial t} + \nabla \cdot \mathbf{\Gamma}_e = S_e \qquad \text{(Continuity)}, \tag{1}$$

$$\mathbf{\Gamma}_e = -\mu_e \boldsymbol{E} - \nabla(n_e D_e) \qquad \text{(Flux–DD)}, \tag{2}$$

$$\frac{\partial(n_e \varepsilon_e)}{\partial t} + \nabla \cdot \left(\frac{5}{3}\varepsilon_e \mathbf{\Gamma}_e - \frac{2}{3}\kappa \nabla \varepsilon_e\right) = -e\mathbf{\Gamma}_e \cdot \boldsymbol{E} - n_e \varepsilon_c \nu_{iz} \qquad \text{(Energy)}, \tag{3}$$

Ions:

$$\frac{\partial n_i}{\partial t} + \nabla \cdot \mathbf{\Gamma}_i = S_i \qquad \text{(Continuity)}, \tag{4}$$

$$\frac{\partial}{\partial t}\mathbf{\Gamma}_i + \nabla \cdot (\mathbf{\Gamma}_i \boldsymbol{u}_i) = \frac{Z_i e n_i}{M_i}\boldsymbol{E} - \frac{\nabla(n_i T_i)}{M_i} - \nu_{iN}\mathbf{\Gamma}_i \qquad \text{(Flux)}, \tag{5}$$

Field:

$$\nabla \cdot (\epsilon \nabla \phi) = -e(Z_i n_i - n_e) \qquad \text{(Poisson)}. \tag{6}$$

Here e is the elementary charge; $Z_i e$ the charge of ion species in units of e; n_e and n_i is the electron and ion densities; $\mathbf{\Gamma}_e (= n_e \boldsymbol{u}_e)$ and $\mathbf{\Gamma}_i (= n_i \boldsymbol{u}_i)$ the electron and ion fluxes; $\boldsymbol{u}_e$ and $\boldsymbol{u}_i$ the electron and ion mean velocities; S_e and S_i the source terms for electrons and ions resulting from collisional and radiative processes (e.g. ionization, recombination, etc); $\mu_e (= e/m_e \nu_{eN})$ and $D_e (= T_e/m_e \nu_{eN})$ the electron mobility and diffusion constants; m_e and M_i the electron and ion masses; ν_{iz} and ν_{eN} the electron ionization and the electron momentum transfer collisional frequencies; ν_{iN} the ion momentum transfer collisional frequency; $\varepsilon_c (= \varepsilon_c(T_e))$ the collisional electron energy loss per electron–ion pair created; $\varepsilon_e (= \frac{3}{2}T_e)$ the mean electron energy; $\kappa (= \frac{5}{2} n_e D_e)$ the scalar thermal conduction coefficient; T_e and T_i the electron and ion temperatures in units of electronvolts; ϕ the electric potential and $\boldsymbol{E} (= -\nabla\phi)$ is the electric field.

The above set of fluid equations, however, is not closed. The average collisional frequencies (e.g. ionization and momentum transfer collisional frequencies) cannot be expressed as a function of only the density, mean velocity and mean energy of each species. Determining these frequencies requires averaging over the particle velocity or energy distribution:

$$\nu = \frac{1}{n_{sp}} \int_0^\infty n_N \sigma_{sp,N}(\varepsilon) \varepsilon f_{sp}(\varepsilon) \mathrm{d}\varepsilon, \tag{7}$$

where n_{sp} is the species density, n_N is the neutral gas density, $\sigma_{sp,N}(\varepsilon)$ is the collision cross section as a function of the relative kinetic energy ε between the species and the neutral gas, and $f_{sp}(\varepsilon)$ is the energy probability function of the species. However, the particle energy distribution $f_{sp}(\varepsilon)$ is unknown because only moments of the Boltzmann equation are solved. Therefore, the velocity distribution of each species must be assumed. Obviously, the simulation results depend on the velocity distribution functions that are chosen.

The simplest approach is to assume that charged particles are in local equilibrium with the electric field, i.e. local field approximation (LFA). The implicit assumption in this approach is that the energy gained by charged particles from the electric field is locally balanced by the loss in collisional processes. In this case, the assumed velocity distribution in time and space is the equilibrium velocity distribution of the particles in a uniform dc electric field equal to that at their location and time in the discharge. Therefore, in the LFA, the energy balance equation (3) does not need to be solved and the various frequencies and constants determining the particle generation, transport and loss are expressed as a local function of the reduced electric field $E(\boldsymbol{x})/n_N(\boldsymbol{x})$, where E is the electric field strength. The LFA fails in regions of strong field gradients.

Another common approach is to assume a Maxwellian energy distribution for each species

$$f_{sp}(\varepsilon) = \frac{2}{\pi^{1/2}(T_{sp}/e)^{3/2}} \mathrm{e}^{-\varepsilon/T_{sp}}, \tag{8}$$

where T_{sp} is the temperature of the species. This implies that the collision frequency between particles of the same species is faster than the other processes such as collisions with other species and energy gain from the fields. Other distributions (e.g. Druyvesteyn) might also be considered in a similar way, with a slightly different meaning for the approximation. In this case, the various frequencies determining the particle generation and loss in the continuity equation and the mobility and diffusion constants in the flux equation are expressed as a function of the particle mean energy (temperature) which is determined by solving the energy balance equation. In low-temperature plasmas, however, the species are typically far from thermal equilibrium, and velocity distributions deviate from the Maxwellian (figure 11).

Finally, the velocity distribution can be assumed to be equal to that of a particle swarm in a spatially uniform effective electric field that gives the same mean energy as determined by the energy balance equation. Similar to the LFA case, the various frequencies involved in the generation and loss terms of the continuity equation and other swarm properties are expressed as a function of E_{eff}/n_N. Although the use of swarm parameters coupled with the solution of the electron energy equation capture to some extent non-local effects through the convection and diffusion of electron energy, the limitations in capturing non-local effects in fluid models have been shown in numerous studies [22].

The example set of fluid equations (1)–(6) can incorporate alternative equations and/or additional terms in order to include additional physics (see, e.g. [23, 24]). Fluid equations are solved numerically after converting the set of coupled differential equations into a set of finite difference equations [25]. This step is crucial in solving the problem because the conditions for numerical convergence depend on the scheme used. The Scharfetter–Gummel method [26, 27], first introduced to solve the continuity equation in solid-state devices, is widely used for the spatial discretization of the transport equations [21, 28, 29]. The Scharfetter–Gummel method slightly modifies the given set of equations by incorporating an additional diffusion term that permits the use of relatively large cell sizes which would otherwise result in unstable numerical solutions in regions of high electric fields. Implicit discretization of the time derivatives is typically employed to overcome the time step limitation restricted by the Courant–Friedrichs–Lewy condition [25].

2.1.2. Strengths and limitations. The major approximation made in fluid models is the assumption of a specific velocity distribution based on the local value of the electric field. Hence, fluid codes are not capable of capturing non-local particle kinetics. Therefore, fluid simulations are more suitable for high pressure discharges where non-local effects tend to be less important due to the very frequent collisions between particles. Nevertheless, non-local phenomena can occur even in high pressure discharges if the electric field is large [30]. Examples of this situation include cathode fall regions and micro-discharges.

Despite this limitation, fluid models are widely used because of their advantage in computational speed. Two- and three-dimensional fluid simulations can be run in a reasonably short time. Additionally, a large number of species can be modelled allowing the study of complicated chemistries with numerous reactions. These problems are more difficult to treat using PIC codes.

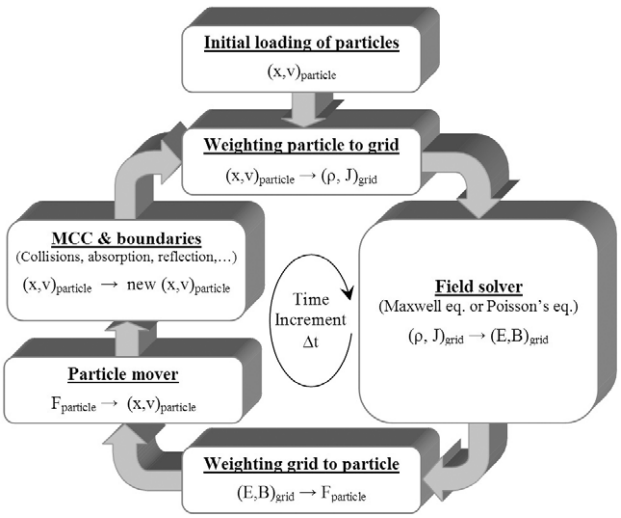

Figure 1. Flow diagram of a PIC-MCC model.

2.2. PIC-MIC models

2.2.1. Description. PIC simulations take advantage of the collective behaviour of charged particles in plasmas to model the kinetics of various species by simulating a reduced number of computer particles (also called super-particles) [2, 3, 31]. Despite the reduced number of particles that are simulated (typically one super-particle per 10^{5-7} real particles in one-dimensional simulations), it was shown in the early days of particle simulations that plasma physics are retained by this simulation technique (see Birdsall [16] and references within). Since super-particles are tracked by solving fundamental equations (Newton–Lorentz equation for the motion of charged particles coupled with Maxwell equations for the self-consistent calculation of electric and magnetic fields) without making any assumption on their velocity distribution, the kinetics of each species are simulated with very little approximation. Typically, electrons and ions are simulated and background neutrals are assumed to be uniformly distributed in space. Boundary conditions imposed by external circuits can be self-consistently considered by solving the Kirchhoff circuit equations simultaneously with Maxwell equations [19]. A detailed review and recent advances in PIC simulations can be found in [32].

A typical flow diagram of a PIC simulation is shown in figure 1. Particles are initially distributed in the simulation domain and in velocity space, and Maxwell equations are solved to determine the electric and magnetic fields self-consistently. Field quantities are solved at grid points whereas particles are allowed to fill the continuum phase space within the simulation domain. In each time step, the position and velocity of particles are updated in time by solving the Newton–Lorentz equation. This requires estimating the fields at each particle position by weighting the field values known at the grid points. Once particles are advanced, collisions are incorporated in the simulation by applying an MCC scheme. The MCC module determines statistically the particles undergoing collisions and their scattered velocities. The interaction between the surface and particles is also modelled at this time by incorporating the reflection, absorption and emission of particles at the boundaries. Maxwell equations (or Poisson's equation in electrostatic simulations) are then solved to determine the self-consistent fields. This step is performed after the charge density is determined by weighting the particle densities onto the grid where the fields are calculated. Once the fields have been calculated, time is advanced and the next iteration begins.

Although grids and interpolations are typically used in computational methods, the weightings of particles to grid points and of fields to particle locations add a new significance to the grid and the weighting schemes. Several techniques have been used and analysed in the past [33–36] and, as a compromise between computer efficiency, physical representation and simulation noise, a linear-weighting is typically chosen in PIC simulations. Although the PIC method significantly underestimates the short-range Coulomb interaction between charged particles within a cell, PIC simulations are computationally faster than the direct solution of Coulombs law [2].

In PIC-MCC simulations, statistical processes are modelled in more detail than in fluid simulations. Differential cross sections for collisions and the energy and angular dependence of secondary electron emission processes at the boundaries can be easily implemented in PIC-MCC simulations. Despite their advantage in terms of kinetic fidelity, PIC-MCC simulations require long simulation runs. Tracking 10^{4-6} particles is computationally very demanding. Given the large number of super-particles that are simulated, the computation of the collision probability of every super-particle in each time step requires a lot of resources. To speed up the collision simulation, a fictitious collision (the so-called null-collision) is added to the collisional processes being modelled [37,20]. The cross section of this null-collision is chosen such that the total collision frequency for each species becomes uniform in space and independent of the energy of the incident particle. Therefore, the collision probability of each particle is the same, and particles undergoing collisions can be randomly selected without computing the collision probability of every super-particle at each time step.

For stability and accuracy, restrictions on some numerical parameters such as cell size Δx and time step Δt need

to be considered [16, 38]. The cell size should generally be smaller than the shortest characteristic length scale of the plasma, i.e. Debye length, sheath length and Larmor radius. The time step should generally be smaller than the shortest characteristic time scale of the plasma, i.e. inverse of plasma frequency, RF driving frequency and maximum collision frequency. The particle Courant condition $v\Delta t/\Delta x < 1$, where v is the particle velocity, should also be satisfied for all particles. And an additional constraint in PIC-MCC simulations is imposed by the statistical description of collisional processes. The time step generally needs to be kept small enough to prevent particles from undergoing more than one collision in one time step. This requirement is satisfied if $\Delta t \nu_{max} \ll 1$ where ν_{max} is the maximum collision frequency of the particles. In order to obtain meaningful results at steady state, simulations for RF discharges are typically run for several thousands of RF cycles requiring long simulation runs.

2.2.2. Strengths and limitations. The major limitation of PIC-MCC simulations is the computation time. This is proportional to the number of super-particles and it is therefore desirable to keep the number of super-particles as low as possible. A number of issues, however, need to be considered when selecting the number of super-particles.

(1) Sufficient statistical representation of energetic particles: for example, in a Maxwellian distribution of 2 eV the number of particles with 20 eV is four orders of magnitude lower than the number of particles with 2 eV. Therefore, a sufficiently large number of particles needs to be simulated to properly represent processes that involve high-energy particles, such as excitation and ionization processes.

(2) Noise: since the plasma behaviour is modelled by simulating a reduced number of computer particles (N), PIC-MCC simulations are intrinsically noisy. The noise is inversely proportional to the square root of N. There is, however, a practical limitation on noise reduction that can be achieved by increasing the number of super-particles. Some alternative techniques such as high frequency or short wavelength filtering have been developed to reduce the noise level [2]. In this case, however, one needs to pay attention to the kind of physics that may also be filtered.

(3) Numerical heating: particles may gain or lose energy due to the numerical heating associated with the noise level in the simulation [39,40]. A sufficiently large number of particles is needed to keep this non-physical energy exchange negligible during the duration of the simulation. As a compromise between numerical accuracy and computational speed, the number of super-particles per cell is typically kept between a few particles up to hundreds of particles. However, when particles in the discharge are trapped for long periods of time, thousands of particles per cell may be required to prevent numerical heating. Figure 2 shows the electron density and temperature in an argon capacitively coupled discharge as a function of the number of super-particles per cell obtained from a one-dimensional PIC-MCC simulation [41] using XPDC1 [16, 19, 20]. Since the electric field in the bulk plasma where low-energy electrons are confined for a long time is small, numerical fluctuations in the electric field value lead to a significant non-physical heating of low-energy electrons. These fluctuations, however, have a less marked effect on high-energy electrons, which are mainly heated in the sheaths where large electric fields exist. For the case shown, it can be seen that over a thousand super-particles per cell are needed to minimize this numerical artefact.

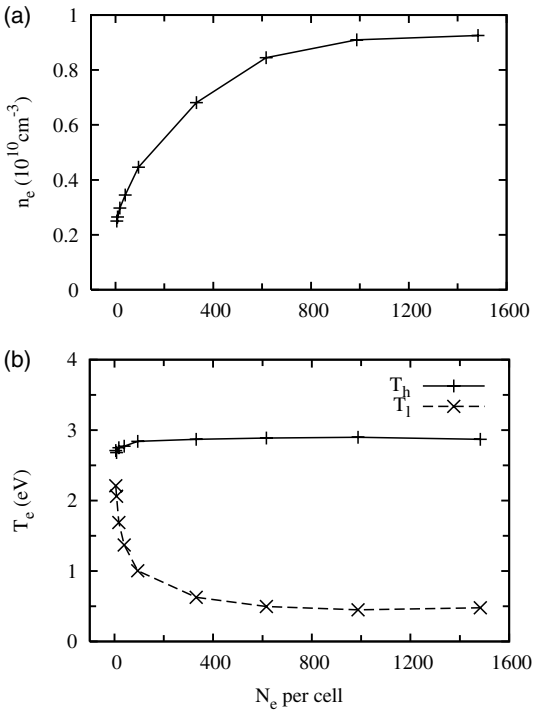

Figure 2. (*a*) Electron density and (*b*) electron temperatures in the bulk plasma as a function of the number of super-particles in a cell. T_h and T_l represent the effective temperatures of high- and low-energy electrons, respectively.

Due to these constraints on the number of super-particles, PIC-MCC simulations are computationally more demanding than fluid simulations. The large number of particles needed to simulate each species limits in practice the number of species that can be modelled. For this reason, PIC-MCC simulations are normally not used when simulating low-temperature discharges with complex chemistry that involves numerous species. Nevertheless, since fundamental equations are solved with few approximations, kinetics of the simulated species can be accurately modelled, including both local and non-local effects. Therefore, PIC simulations are well suited for low pressure discharges where non-local effects can be very important, particle densities are low and the MCC scheme can be solved relatively quickly.

Finally, it should be mentioned that various techniques have been developed to speed up PIC-MCC simulations. These techniques include implicit movers, longer ion time steps, lighter mass ions, different weights for electrons and ions, non-uniform initial density profiles, different weights for low- and high-energy particles and code parallelization [38,42,43]. Although simulation time can be drastically reduced in some cases by a combination of these techniques, PIC-MCC codes remain typically slower than fluid codes.

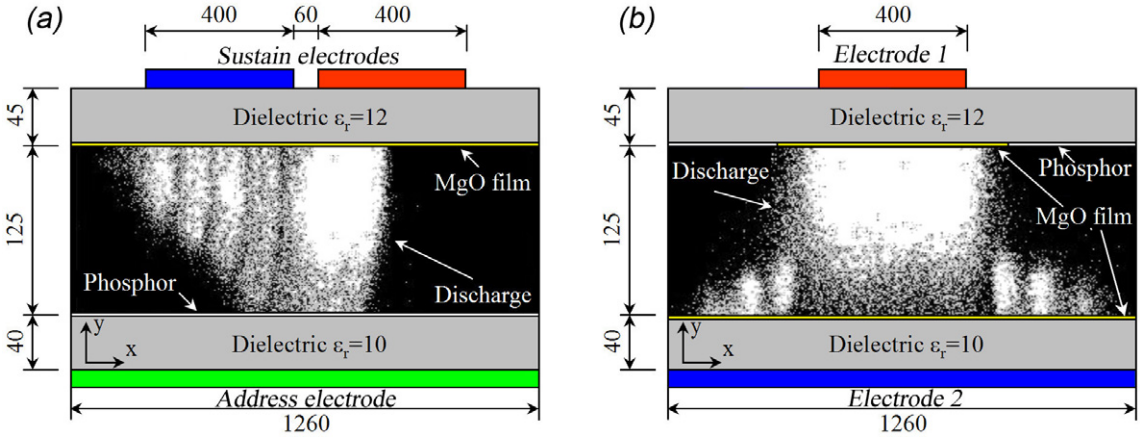

Figure 3. Two-dimensional schematic of (*a*) coplanar- and (*b*) matrix-type PDP cells. Dimensions are given in micrometres and figures are not drawn to scale.

2.3. Hybrid models

Hybrid models are a combination of fluid and PIC models. The idea behind hybrid models is to get a model that outperforms both fluid and PIC models by combining the fast speed of fluid simulations with the accurate particle kinetics of PIC models. The end result is that hybrid codes run faster than PIC codes yet are slower than pure fluid codes, and describe some kinetics more precisely than fluid models.

Depending on the physics to be modelled, various hybrid models can be derived. Ions can be modelled as a fluid while electrons are treated in a PIC scheme [44]. Alternatively, only high-energy electrons can be tracked in a PIC scheme while ions and low-energy electrons are treated as fluids [29, 45]. To study the energy distribution function of ions impacting on a wafer in semiconductor processes, ions may be simulated using a PIC scheme while electrons are considered a Maxwellian fluid [46]. In fact the design of a hybrid model depends on the particular physics to be captured.

One of the critical steps in implementing hybrid codes is the communication between the fluid and the particle parts. Time step requirements are in general quite different in the fluid and particle simulations. This is the same problem that is faced when physics occurring at different time scales are included in the same model. One approach to overcome this difficulty is to use the smallest time step required for either of the modules. This approach captures the transient behaviour of the plasma although a long simulation time is required. Often, however, we are interested only in the steady state solution. In this case, simulation time may be drastically reduced by predicting the plasma properties at a future time based on the recent evolution of the discharge. By considering educated predictions, simulation time can be drastically reduced at the cost of losing the transient behaviour.

3. Plasma display panels

In recent years, PDPs have become an alternative to conventional cathode ray tubes (CRTs) for large screen applications. The size of current PDPs ranges between 40 and 80 inches with very small thickness in comparison with CRTs. PDPs offer a wide viewing angle ($>160^{\circ}$), a high colour resolution and a fast response time [47,48]. Despite continuous development and increase in market share, however, PDP luminous efficiency remains low ($\sim 1.5\,\mathrm{lm\,W^{-1}}$). In order to meet the challenges imposed by existing and promising new technologies like liquid crystal displays and field emission displays, a substantial effort is being made to improve the efficiency of PDPs and reduce their fabrication cost. Different gas chemistries, cell geometries, operating pressures and driving schemes are being investigated.

Experimental diagnostics of PDP cells are not trivial. The small dimensions of a PDP cell (~ 1 mm) and the short life of the discharge ($\sim 1\ \mu$s) limit the diagnostic techniques that can be employed and the resolution that is achieved. For these reasons, computer simulation has become a very valuable means of understanding the discharge behaviour in a PDP cell and of revealing its underlying physics. Despite the limitations of fluid simulations (section 2.1), this simulation technique has been extensively used in studies of PDP cells because of its fast simulation time [49–51]. Fluid simulations have been performed to analyse new designs aimed at improving the luminous efficiency of PDP cells as well as to investigate the underlying physics of the discharge [52]. In order to model the luminous efficiency accurately, a self-consistent radiation transport model of the UV emitted by the excited species is required [24, 53]. Although most PDP simulations are two-dimensional, three-dimensional simulations are needed to optimize parameters such as the height and position of the barrier ribs and the shape and area of the electrodes [54–56]. PIC simulations have also been performed to investigate kinetic effects in PDP cells [57, 58].

Schematics of two common types of PDP cells (coplanar and matrix types) are presented in figure 3. The PDP cell is a dielectric barrier micro-discharge [59] and its principle of light emission is analogous to that of a fluorescent lamp, i.e. UV emitted by excited species is converted into visible light by a phosphor. The most common types of cells are the ac PDP cells as they outperform the early dc cells. Electrodes are separated from the discharge by a thick transparent dielectric, and a thin layer of MgO is deposited on the plasma side of the dielectric. The discharge is ignited by applying a sufficiently high voltage between two sustain electrodes. In a coplanar-type PDP cell, both electrodes are placed on the

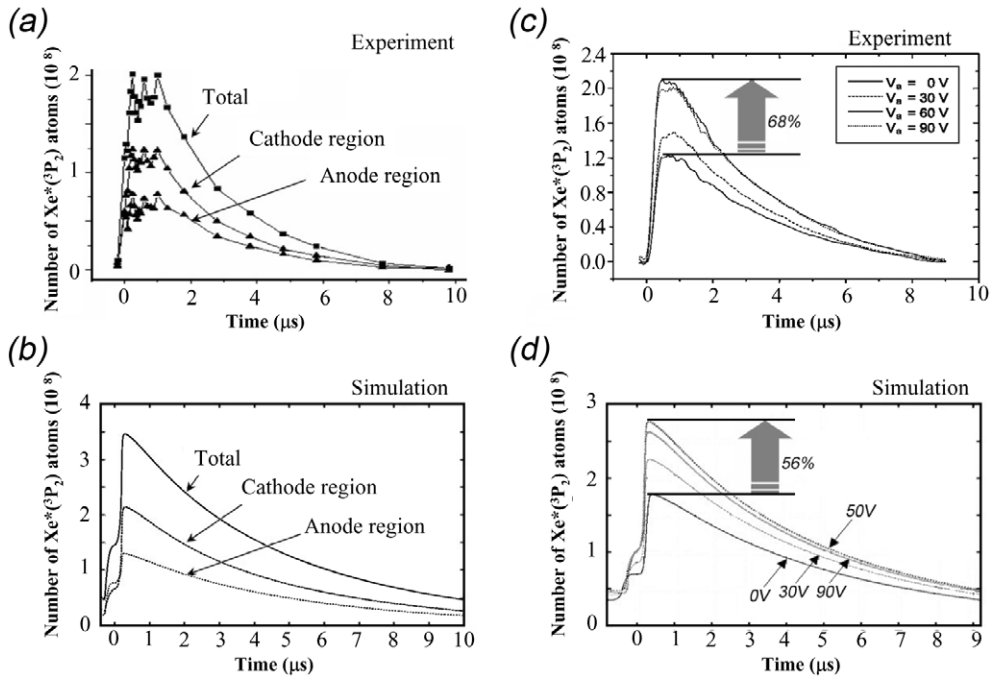

Figure 4. Comparison between experimental measurements ((*a*) and (*c*)) and simulation results ((*b*) and (*d*)) in a coplanar PDP cell. (*a*)–(*b*) Number density of $Xe^*(^3P_2)$ atoms in the anode and the cathode regions when the conventional driving pulse scheme is used. (*c*)–(*d*) Total number density of $Xe^*(^3P_2)$ atoms when pulses of different amplitude are applied to the address electrode. (*a*) Reprinted with permission from [60], copyright 2003 IEEE. (*b*) Reprinted with permission from [61], copyright 2003 IEEE. (*c*) Reprinted with permission from [56], copyright 2004 Wiley-VCH. (*d*) Reprinted with permission from [62], copyright 2003 KIDS.

upper dielectric, whereas in the matrix-type they lie on opposite sides of the cell (figure 3). The voltage required to ignite the discharge, i.e. the breakdown voltage, depends on the amount of surface charge pre-accumulated on the dielectrics. Thus, by controlling the amount of surface charge that accumulates during the address period, it is possible to selectively turn on cells in the subsequent sustain period. The maximum operating voltage used in the sustaining period is limited so that only cells with pre-accumulated surface charge can ignite.

The electronics associated with the driving circuit of PDPs have to be capable of generating high voltages and fast pulses. In order to reduce the cost of the driving circuit, it is desirable to keep the driving voltage as low as possible. This imposes some constraints on the gas used in PDP cells. Typically PDP cells operate with mixtures of noble gases at a pressure of the order of hundreds of Torr. Xe gas is used for its high UV radiation efficiency and low visible light emission. However, since Xe ions are inefficient at generating secondary electrons when impinging on the MgO layer, a high voltage is required to ignite a pure Xe discharge. In order to lower the driving voltage, buffer gases (Ne, He, etc) having high secondary electron emission coefficients are typically mixed with Xe. To improve the efficiency and luminance of the cell, high Xe concentration (∼10%) and complex gas mixtures are being investigated.

3.1. Benchmark of fluid simulations in PDP cells: excited Xe species density

One of the key parameters in the performance of PDP cells is the density of the excited Xe species. UV photons (with wavelengths of 147, 150 and 173 nm) emitted from Xe excited states are converted to visible photons by the phosphor covering the cell walls. Simulation results indicate that only ∼15% of the input energy to a PDP cell is spent in creating excited species [24]. This low percentage is one of the main limitations in the overall efficiency of the PDP. In order to predict luminous efficiency by computer simulations, it is necessary to accurately model the generation and loss of these excited species.

Despite the difficulty in diagnosing an actual PDP cell, Tachibana and co-workers [60, 61] have recently measured the spatio-temporal behaviour of excited Xe atoms experimentally by means of laser absorption spectroscopy. Two- and three-dimensional fluid simulation results have been compared with their experimental data by Yang *et al* [56, 62]. The same gas composition, pressure and driving voltage scheme used in the experiments were used in the simulations. Secondary electron emission coefficients at the boundaries depended on the incident particle species and the surface material. In the simulations, secondary electron emission coefficients for Ne and Xe ions impinging on the MgO layer were assumed to be 0.5 and 0.05, respectively. For the excited species and molecular ions of Ne and Xe, the same secondary electron emission coefficients as their atomic ions were used. Chemical reactions of the molecular ions Xe_2^+, Ne_2^+ and $NeXe^+$ were taken into account and a modified Holstein's equation [24, 53] was used to self-consistently model the resonant excited species $Xe^*(^3P_1)$. The modified Holstein model is more accurate than the conventional effective trapping factor method [54] because the spatial redistribution of $Xe^*(^3P_1)$ is taken into account.

Figure 4 shows the time evolution of the number density of Xe metastables ($Xe^*(^3P_2)$) during one driving pulse.

The simulation results of Yang *et al* are compared with the measured data of Tachibana *et al*. Although there are some discrepancies in the absolute values, the order of magnitude and trends of the simulation results are in good agreement with the experimental measurement. Sixty per cent of the Xe excited atoms are found in the cathode region and the peak Xe density decays to half its value in 2–2.5 μs in both simulation and experiment (figures 4(*a*)–(*b*)). The time and spatial density distributions also show good agreement [62]. When non-conventional pulses are applied to the address electrode (figures 4(*c*)–(*d*)), higher densities are obtained due to the pre-ionization of the gas. Good agreement is also found between the simulation results and experimental measurements under these conditions. In both experiment and simulation, a maximum density is obtained when the amplitude of the address electrode pulse is 50–60 V.

Reducing the uncertainty of plasma parameters (such as secondary electron emission coefficients and gas reaction rates) and eliminating several assumptions (such as the LFA) can lead to better agreement between simulations and experimental measurements. These validations, however, justify the use of simulation as an aid in the design of these devices. Using fluid simulations, new cell structures and alternative driving schemes for high luminous efficiency can be studied.

3.2. Charged particle kinetics in PDP cells

Although fluid simulation is a useful tool for providing insight into the physics of PDP discharges and suggesting new cell designs, fluid models do not provide accurate kinetic information. In order to obtain such information without making *a priori* assumptions regarding the particle velocity distributions, PIC-MCC simulations are indispensable.

3.2.1. Ion kinetics: ion angle and energy distributions. One of the main concerns in PDPs is the lifetime of the MgO thin layer. This ~0.5 μm thick film plays a key role in igniting the discharge. It protects the dielectric from the bombardment of energetic particles and provides a high yield of secondary electrons. The erosion of the MgO layer due to ion bombardment is therefore of major consequence for the lifetime of the PDP. PIC-MCC simulation is a valuable tool for studying the erosion of this film by identifying the main species contributing to the bombardment and the angle and energy distributions of incident particles.

Despite the importance of the secondary electron emission coefficient of the MgO layer in the overall performance of a PDP cell, its exact value remains undetermined. There exist discrepancies in several experimental and theoretical results [63, 64]. Furthermore, experimental conditions do not often represent the actual bombardment occurring in a PDP cell. It is expected, for example, that ions in a coplanar PDP cell do not impinge perpendicularly on the MgO surface. Simulation results can be used to design new experimental set-ups to measure secondary electron emissions under more representative conditions. In addition, using the ion angle and energy distributions, the erosion profile of the MgO thin layer due to incident ions can be estimated.

PIC-MCC and hybrid simulations can reveal the energy distribution function of ions and fast neutrals incident on the MgO layer in PDP cells [48, 58, 65, 66]. Simulation results indicate that ions impinging on the MgO layer have an average energy which is ~10% of the applied voltage. Yang *et al* [56, 67, 68] have obtained the energy and angle distribution functions of impinging ions by means of a two-dimensional PIC-MCC simulation (XOOPIC [69]). Some of their results are presented in figure 5.

From the results shown in figure 5, it is evident that experiments performed with energetic ions bombarding a target perpendicularly are not representative of the conditions encountered in an actual PDP cell. In the case of a coplanar cell, the average incidence angle measured with respect to the normal direction to the MgO layer is ~15°. This average angle reduces to around 3° for the case of a matrix cell. The wide angle distribution observable in figures 5(*a*) and (*b*) is a consequence of electric field direction and the numerous collisions of ions with neutrals. Motivated by these simulation results, experimental measurements of the secondary electron emission coefficient have been recently performed with an ion beam incident on the surface at tilted angles [70]. The measurements, however, were limited to ion-beam energies larger than 80 eV and incidence angles only up to 30°.

The ion energy distributions of Ne and Xe (figures 5(*c*) and (*d*)) are Maxwellian. In spite of a high driving voltage (300 V), most ions have energies of less than 30 eV because of frequent collisions with neutrals. The resonant charge exchange collision between ions and their parent neutrals is the most frequent collision. Since the fraction of Ne is typically much larger than that of Xe, Ne ions are more likely to undergo resonant charge exchange collisions than Xe ions and as a result, Ne ions hit the MgO surface with lower energies than Xe ions. However, when the Xe concentration increases, the high-energy tail portion of the Xe ion energy distribution reduces while that of Ne ions increases (figure 5(*d*)). These trends of ion energy distributions obtained using a PIC-MCC model are analogous to the simulation results from hybrid models [48, 65, 66].

3.2.2. Electron kinetics: striation formation. PIC-MCC simulations of PDP cells also provide information regarding electron kinetics. By means of two-dimensional PIC-MCC simulations, Iza *et al* have recently shown that despite the high operating pressure, non-local electron kinetics plays a key role in the formation of striations in PDP cells. They propose a mechanism for the striation formation based on the combined effect of surface charge accumulation on the anode dielectric, a well-like deformation of the spatial potential profile and non-local kinetics of low-energy electrons [30]. The model agrees with experimental observations of striations forming along the anode dielectric in various PDP cell configurations [71, 72]. Figure 3 shows the simulated ion density in coplanar and matrix cells, once striations have formed. Since resolving striations in time and space experimentally is not trivial, limited experimental data exist and simulations are of great value in understanding the underlying discharge physics.

Despite the success of fluid simulations in describing and predicting the performance of PDP cells, non-local effects cannot be described by this simulation technique (section 2.1). Figure 6 shows a comparison of the simulation results obtained

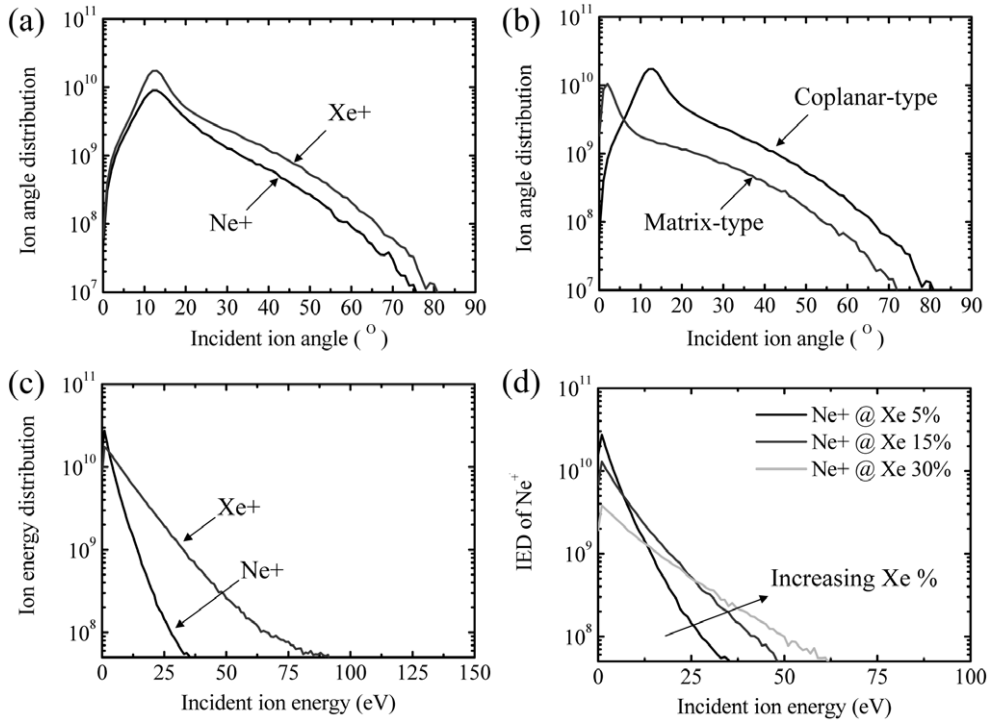

Figure 5. Kinetic information of ions impinging on the MgO surface in the cathode region when the cells are driven at 300 V in a 95% Ne–5% Xe mixture with 300 Torr: (*a*) angle distributions of Ne ions and Xe ions, (*b*) comparison of Xe ion angle distributions in matrix- and coplanar-type PDP cells, (*c*) energy distributions of Ne ions and Xe ions and (*d*) Ne ion energy distributions for different Xe concentrations.

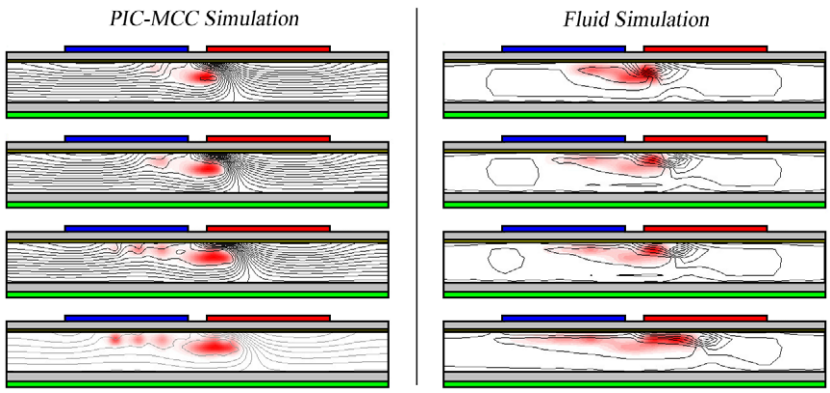

Figure 6. PIC-MCC and fluid simulations of a coplanar PDP discharge at 500 Torr in a mixture of 4% Xe–96% Ne. Lines represent equipotential contours and shading electron density. Reprinted with permission from [73], copyright 2001 American Institute of Physics.

by Shon and co-workers [73, 74] using two-dimensional PIC-MCC and two-dimensional fluid codes. Striations are clearly identified in the PIC-MCC simulation results but smear out in the results obtained with the fluid code due to the LFA. The formation of striations can be explained in terms of non-local kinetics of low-energy electrons. Although non-local effects are normally not observed at pressures above a Torr, it is the reduced electric field E/n_N and not the pressure that determines the locality of the electron velocity distribution [75]. The small dimension of PDP cells results in a large electric field that accounts for the non-locality of low-energy electrons even at the high pressures encountered in PDP cells.

Simulations performed on the coplanar and matrix geometries depicted in figure 3 show that striations form even when no surface charge is present on the dielectrics at the beginning of the discharge [30]. Therefore, pre-existing surface charge is not responsible for the striation formation. Simulations results and experiments in cells with bare electrodes, however, indicate that striations do not form if charge is not accumulated on the dielectric covering the anode [30, 71].

Figure 7 shows the spatial potential evolution along a plane parallel to the anode dielectric 15 μm inside the cell when a pure Ne discharge is sustained in coplanar- and matrix-type PDP cells by an applied voltage of 350 V. As indicated in the figure, the location where striations appear can be predicted by the potential profiles. The potential difference between the locations of consecutive striations corresponds to the ionization potential of the gas (22 V for Ne in this case). This indicates that the electron energy is given by the potential

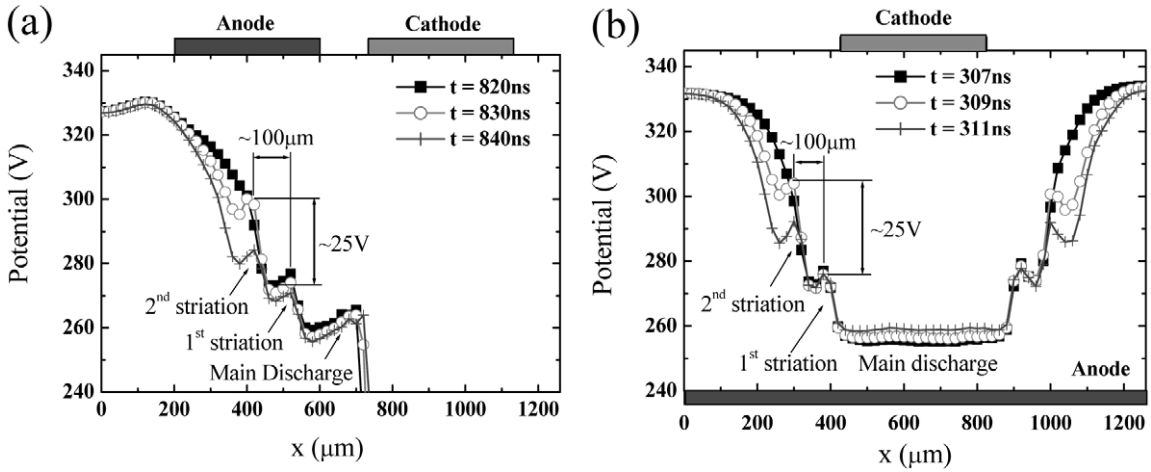

Figure 7. Time evolution of the spatial potential distribution in the anode region of a pure Ne discharge at 500 Torr (*a*) in a coplanar PDP cell and (*b*) in a matrix PDP cell. Potentials lines plotted for a plane parallel to the anode dielectric at a distance of 15 μm.

distribution and not the electric field, i.e. electrons are not in local equilibrium with the field.

4. Capacitively coupled plasmas

Capacitively coupled plasmas (CCPs) operating at RF have been extensively studied during the last decade or so because of their widespread applications [76–80]. Analytical and numerical models and experimental measurements have led to a substantial understanding of the physics underlying these discharges.

A CCP reactor consists of two parallel electrodes separated by a small gap (typically a few centimetres) where the discharge is ignited. In a conventional single-frequency CCP, one electrode is kept at ground potential while the other is connected to an RF power generator. The typical frequency used is 13.56 MHz, an RF band reserved for industrial applications. In a CCP, the electric field sustaining the discharge is perpendicular to the electrodes, and large sheaths form around them. This results in energetic ion bombardment of the electrodes, which can not only damage the electrodes or wafers sitting on them but also limits the overall efficiency of the discharge. As higher power is put into the discharge, the sheath voltage and hence the ion bombardment energy increases. This eventually limits the maximum density achievable with this plasma source.

Although increasing the excitation frequency would result in better power efficiency [81], the main limitation of a CCP reactor is the difficulty in independently controlling the plasma density and the sheath potential, i.e. the flux and energy of the ions striking the wafer. This limitation has favoured the use of alternative sources (e.g. ICP sources, dual-frequency CCP, etc) where higher density and independent control of density and energy can be achieved.

In their favour, CCP reactors present good uniformity thanks to the parallel plate configuration. This is critical in semiconductor applications where strict uniformity requirements have to be met. In order to improve the controllability of CCPs, dual-frequency CCP reactors have been developed [82–86]. The use of two power sources operating at different frequencies allows better control of the electron and ion energy depositions. In a simplified picture, the plasma density and thereby the ion flux is controlled by the high-frequency power, and the ion bombardment energy is determined by the low-frequency power. In reality, however, the control is not independent as both sources influence the electron temperature and sheath potentials in the discharge [87, 88]. The frequency used in the high-frequency source typically ranges from 13.56 MHz up to hundreds of megahertz while the low-frequency source ranges from a few megahertz up to 13.56 MHz.

For typical semiconductor applications (etching, deposition, etc), CCPs are operated at a pressure below a few hundred milliTorr to maintain ion-collisionless sheaths. This is necessary in order to achieve anisotropy in etching processes, a typical characteristic of plasma processes not achievable with wet techniques. At this low pressure, the electron mean free path becomes comparable to the chamber size and non-local electron kinetics is indispensable to explain the discharge characteristics. In the early days of CCPs it was found experimentally that discharges could be sustained even at pressures where the electron–neutral collisional frequency was much lower than the excitation frequency. Under this condition, ohmic heating is very inefficient and cannot justify the existence of the discharge. While low-energy electrons are confined to the bulk of the discharge by the ambipolar electric field created between the electrodes, high-energy electrons can escape this potential well and interact with the high electric fields present in the sheath regions. These interactions lead to a variety of non-local effects that have been reported in the literature [17, 18, 89–91].

Since non-local electron kinetics plays a key role in low-pressure CCP discharges, PIC-MCC models are better suited than fluid models for studying these discharges. Figure 8 shows a comparison between fluid and PIC-MCC simulation results in a symmetric CCP reactor. The one-dimensional fluid and PIC-MCC models are based on a swarm electron velocity distribution and XPDP1 [16, 19, 20], respectively. Striking differences can be observed between the two simulation results indicating the limitations of the fluid approach for modelling low-pressure CCP discharges. Since this fluid simulation uses the DD approximation for electrons, the momentum relaxation

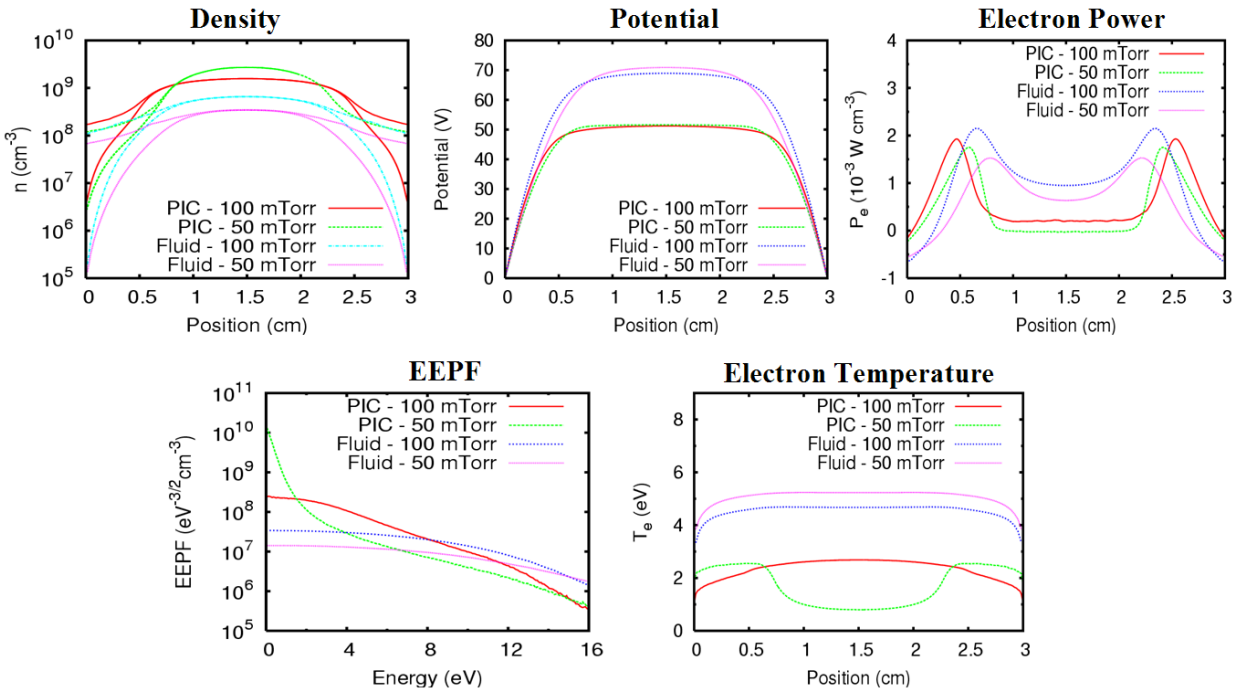

Figure 8. Comparison between one-dimensional fluid and PIC-MCC simulation results of argon discharges in a symmetric CCP reactor with an electrode separation of 3 cm operated at 100 V and 13.56 MHz. The density profiles include both electron and ion densities.

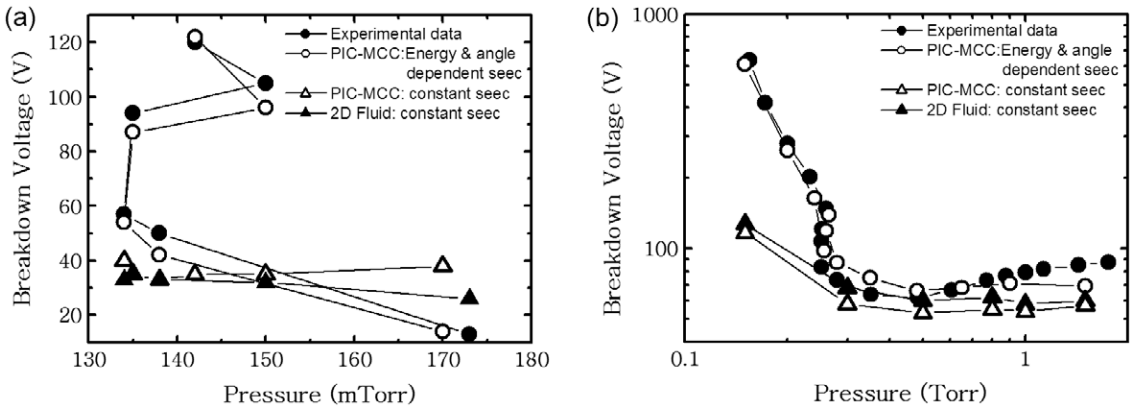

Figure 9. Breakdown voltage (rms) as a function of gas pressure for argon discharges: (*a*) at 27 MHz in a gap of 1.6 cm—experimental data obtained from [93] and (*b*) at 13.56 MHz in a gap of 1.4 cm—experimental data obtained from [94].

effect under the gas pressure of 50 mTorr could change the density and potential profiles quantitatively. The simulation results shown correspond to argon discharges sustained in a gap of 3 cm at 100 V and 13.56 MHz. The secondary electron emission coefficient due to the ion impact was considered constant and set equal to 0.2, and the pressure varied between 50 and 100 mTorr.

Fluid simulations predict lower bulk densities and larger plasma potentials than PIC-MCC simulations. This could lead to an overestimation of the ion energy reaching the wafer when the plasma potential is comparable to the dc self bias in an asymmetric CCP reactor. The main differences, however, are seen in the electron energy probability function (EEPF) in the bulk of the plasma and in the electron power deposition ($P_e = \boldsymbol{J}_e \cdot \boldsymbol{E}$ where J_e represents the electron current) across the discharge. A transition from a bi-Maxwellian to a Druyvesteyn EEPF is observed as the gas pressure increases from 50 to 100 mTorr. This transition is related to non-local electron kinetics and is discussed and compared with experimental data in section 4.1.2. The fluid simulation clearly fails to capture this transition because this model cannot deal with non-local kinetics. PIC-MCC simulations indicate that the power deposited to the electrons (P_e) is mainly deposited at the sheaths with little positive or even slightly negative power deposited in the bulk. This contrasts with the much larger (but incorrect) positive power deposition profile predicted by the fluid simulation.

4.1. Benchmark of particle simulations in CCPs

4.1.1. RF breakdown. The RF breakdown voltage is the minimum sustaining voltage of the RF glow discharge. Figure 9 shows the RF breakdown voltage as a function of pressure for argon discharges in two parallel plate

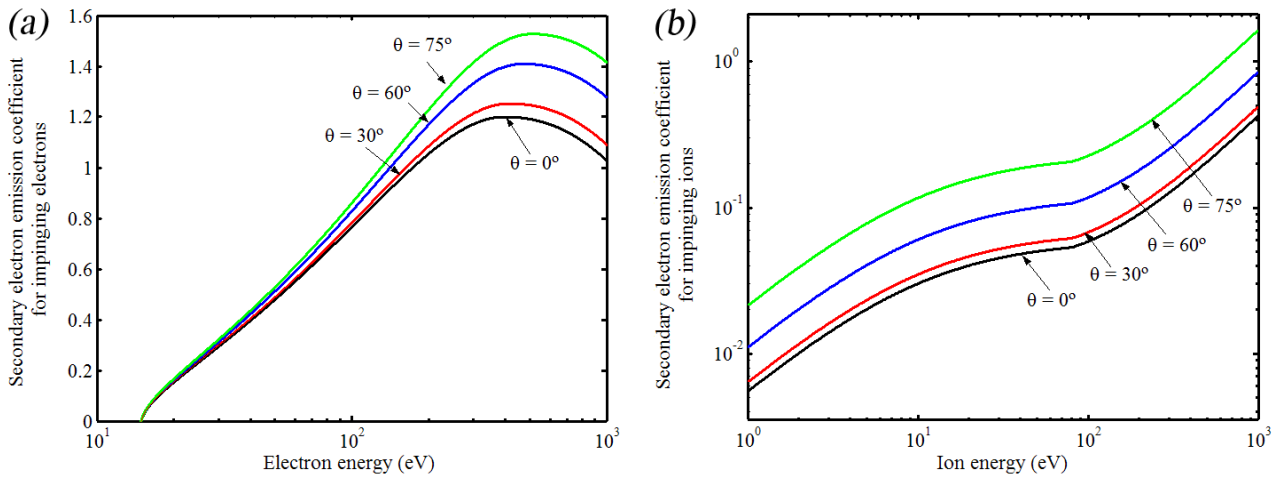

Figure 10. Secondary electron emission coefficient as a function of the energy and angle of the incident particle on a metal electrode: (*a*) incident electrons and (*b*) incident argon ions. The angle is measured with respect to the perpendicular direction to the surface.

systems. Simulation results obtained using various ion-impact secondary electron emission models [92] are compared with experimental data [93, 94]. Simulations were performed using a two-dimensional fluid code with a constant secondary electron emission coefficient of 0.2, a one-dimensional PIC-MCC code (XPDC1) with the same constant secondary electron emission coefficient and a modified XPDC1 code with a secondary electron emission model that incorporates the energy and angular dependence of impinging particles. Excellent agreement is achieved between experiments and simulations when the energy and angular dependences of the secondary electron emission are taken into account. However, significant disagreement is observed at low pressures when the secondary electron emission coefficient is kept constant.

Although secondary electron emission has little effect on the right-hand side of the Paschen curve where the breakdown voltage is determined by the balance between volume generation and diffusion losses, secondary electron emission strongly influences the slope of the left-hand side of the breakdown curve [92, 95, 96]. The modified XPDC1 code used in [92] incorporates Vaughan's model [97, 98] for the secondary electron emission induced by electrons impinging on the electrodes and the electron yield per ion suggested by Phelps *et al* [99, 100] with a secant dependence on the angle of incidence [101, 102]. Figure 10 shows the resulting energy- and angle-dependent secondary electron emission coefficients for incident electrons and ions.

4.1.2. Electron energy distribution functions. Since there are significant discrepancies between fluid and PIC-MCC simulation results in low-pressure CCPs, it is desirable to confirm that PIC-MCC simulations actually reflect the conditions encountered in a real discharge. Figure 11(*a*) shows the electron energy distribution function (EEDF) in an argon CCP discharge measured experimentally by means of a Langmuir probe in a CCP reactor [89]. The EEDF obtained from one-dimensional PIC-MCC (XPDP1) simulations for the same conditions is shown in figure 11(*b*) [103]. The transition from a bi-Maxwellian electron distribution to a Druyvesteyn distribution as the gas pressure increases is clearly captured by the PIC-MCC simulation. This transition is also reflected in the density and electron temperature in the bulk of the plasma (figure 11(*c*)). A rapid decrease in density accompanied with an increase in electron temperature is observed when the pressure increases from 100 mTorr to 1 Torr.

In figure 11(*c*) the simulation results obtained by different authors are compared with the experimental data measured by Godyak and Piejak [89]. Vahedi *et al* [104] and Kim *et al* [103] obtained their results using a one-dimensional PIC-MCC code (XPDP1) while Schweigert and Schweigert [105] used a hybrid model (the so-called combined PIC-MCC approach). The PIC-MCC simulations by Kim *et al* [103] were performed with a number of super-particles four times larger than those used by Vahedi *et al* [104]. Although the transition is captured by all simulations shown in the figure, different levels of accuracy are obtained. As mentioned in section 2.2, the fidelity of a PIC-MCC simulation strongly depends on the number of super-particles used in the simulation (see figure 2). The best agreement with experimental data was obtained by Kim *et al* [103] when a sufficiently large number of super-particles, i.e. 1.5×10^5, was used in the simulation.

4.2. Charged particle kinetics in CCPs

The transport of electrons and ions in the plasma determines the characteristics of the various fabrication processes (sputtering, etching, deposition, etc) performed with CCPs. This kinetic information about charged particles can be obtained by means of PIC-MCC simulations.

4.2.1. Ion kinetics: ion energy distribution function. In order to meet the stringent requirements of modern etch technologies, it is necessary to understand the mechanisms by which ions acquire energy in the sheath and how they deposit it onto the wafer. Ideally, one would like to have full control over the energy and angle distributions of impinging ions and thereby the etching profile. Various authors have studied the ion energy distribution function (IEDF) in single- and dual-frequency CCPs as a function of the applied voltage and the excitation frequency [106–108]. Figure 12 shows some of the

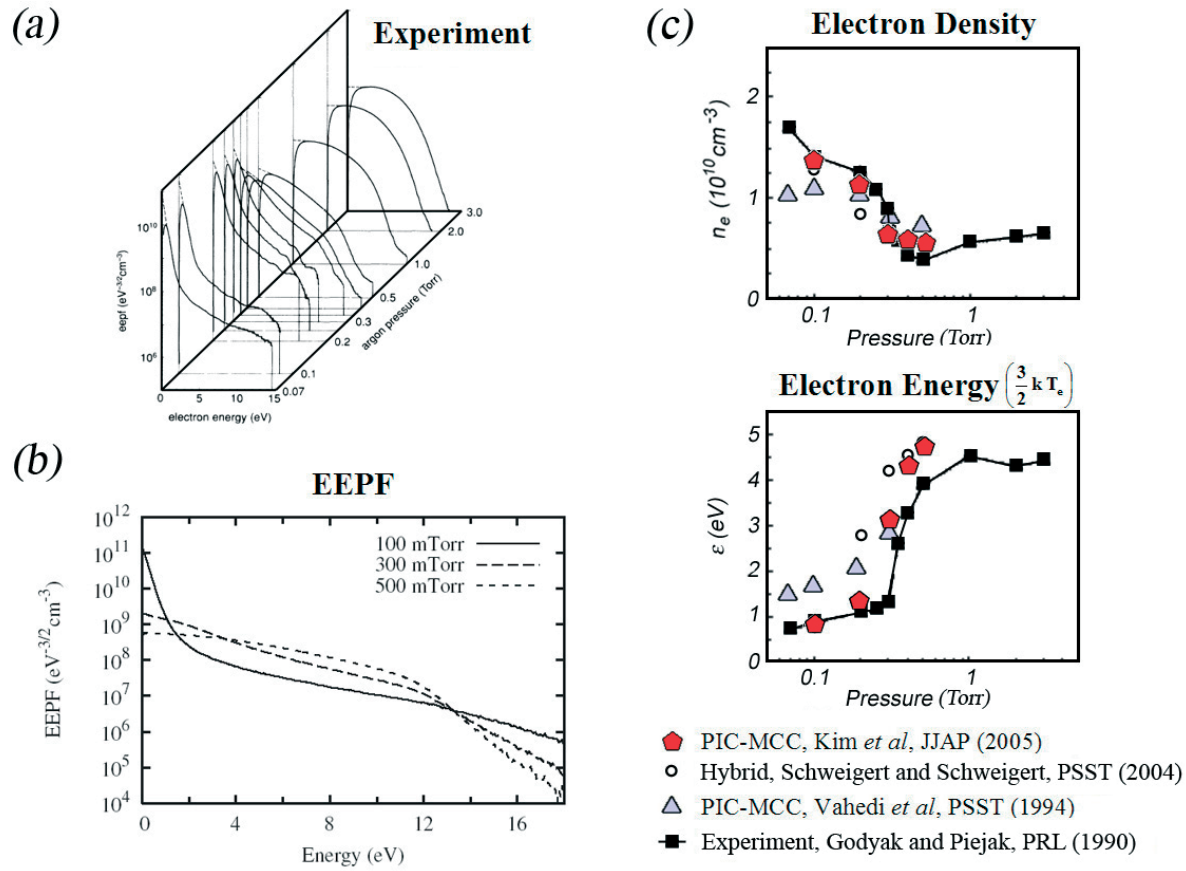

Figure 11. Comparison between (*a*) measured and (*b*) simulated EEDFs, (*c*) electron densities and electron temperatures in an argon CCP discharge. (*a*) Reprinted with permission from [89], copyright 1990 American Physical Society. (*b*) Reprinted with permission from [103], copyright 2005 Japan Society of Applied Physics.

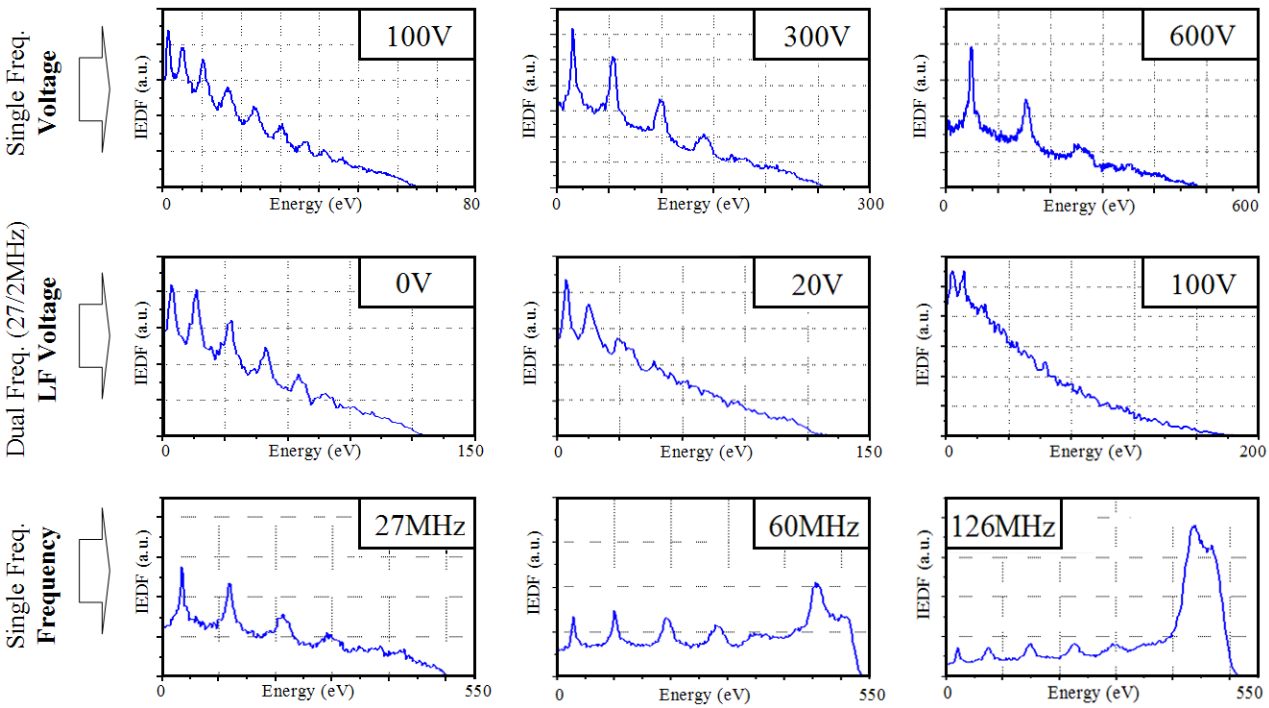

Figure 12. Influence of the voltage, frequency and low-frequency voltage on the IEDF in single- and dual-frequency CCPs. Adapted with permission from [108], copyright 2005 Institute of Physics.

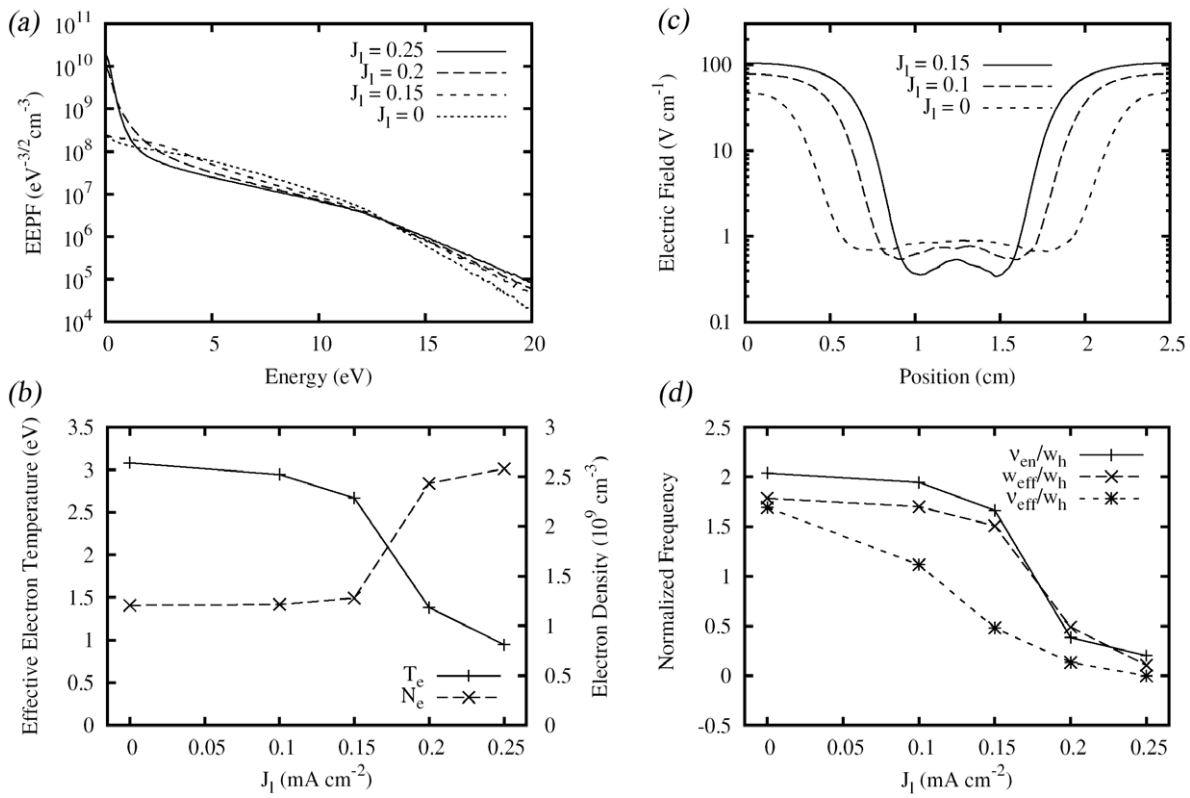

Figure 13. One-dimensional PIC-MCC simulation results for an argon discharge at 100 mTorr in a dual-frequency (27 and 2 MHz) CCP reactor. (*a*) Electron energy probability function. (*b*) Effective electron temperature and electron density in the centre of the discharge. (*c*) Time-averaged spatial profile of the electric field. (*d*) Electron–neutral collision frequency (ν_{en}), effective excitation frequency (ω_{eff}) and effective electron–neutral collision frequency (ν_{eff}) normalized by the high-frequency of excitation in the centre of the discharge (ω_h). Data were presented for various low-frequency currents. Reprinted with permission from [87, 88], copyright American Physical Society.

results obtained by Lee *et al* using a one-dimensional PIC-MCC code (XPDC1) to simulate an argon discharge at 67 and 100 mTorr.

For the conditions simulated, ions undergo collisions as they cross the sheath and the IEDFs extend from virtually zero energy to a maximum that is controlled mainly by the applied voltage. The shape of the distribution is determined by the collisionality of the sheath and the ratio of ion transit time across the sheath to the excitation period. Both factors depend on the excitation frequency. Increasing the excitation frequency from 27 to 126 MHz in a single-frequency argon discharge at 100 mTorr clearly affects the IEDF (figure 12). At 126 MHz the ion sheath transit time becomes much larger than the RF period and the thinner sheath becomes less collisional. This leads to an increase in the number of energetic ions impinging on the electrode.

Since the number of collisions ions undergo as they transit the sheath increases with the sheath width, large voltages and low frequency results in a larger number of low-energy ions. The multiple peaks that appear in the IEDF are due to charge exchange collisions [107–109]. In the case of a dual-frequency CCP, these peaks are smeared out when large low-frequency voltages are applied.

4.2.2. Electron kinetics: mode transition in dual-frequency CCPs. Transitions between α and γ modes [89] and between collisionless and collisional heating [110] are well known in CCPs. These transitions are typically induced by changes in the applied voltage and the operating pressure, and result in abrupt changes in the discharge properties (electron distribution function, effective electron temperature, density, etc). A transition induced by varying the magnitude of the low-frequency current in a dual-frequency CCP has been recently observed in PIC-MCC simulations [87, 88]. Figure 13 shows some of the simulation results obtained for an argon discharge at 100 mTorr in a 27 MHz/2 MHz dual-frequency CCP reactor as the low-frequency current is varied while keeping the high-frequency current constant. Although secondary electron emission can affect the nature of the transition [87, 88], only the case of negligible secondary electron emission is considered here. The electron energy distribution changes from Druyvesteyn to bi-Maxwellian as the low-frequency current increases (figure 13(*a*)). This transition is accompanied by a rapid decrease of the bulk electron temperature and an increase in plasma density (figure 13(*b*)).

The spatial inhomogeneity of the electric field is a key parameter in determining the EEDF shape. The time-averaged electric field as a function of the low-frequency current is shown in figure 13(*c*). As the low-frequency current increases, so does the electric field in the sheath region. The electric field in the bulk region, however, decreases. These variations of the electric field lead to a decrease of the low-energy electron temperature in the bulk of the plasma and an increase in the temperature of the high-energy tail.

Ideally, one would like to control the sheath voltage and width by means of the low-frequency source without affecting the bulk conditions. This would allow independent control of ion flux and energy to a wafer. However, as shown in the electric field profiles (figure 13(*c*)), the low-frequency source also influences the discharge conditions in the bulk plasma.

The effective collision frequency and the effective excitation frequency calculated from the plasma conductivity in the centre of the discharge are shown in figure 13(*d*). The transition which is observed as the low-frequency current increases can be associated with the rapid decrease of these frequencies. As the low-frequency current increases, the sheaths widen and the electron mean free path becomes larger than the size of the bulk plasma. This triggers a series of collisionless effects in the discharge. As shown in figure 13(*d*), the effective collision frequency in the discharge is smaller than the actual electron-collision frequency. The difference between the actual frequencies and the effective frequencies shows the significance of non-local effects (neglected in fluid models).

5. Inductively coupled plasmas

ICP reactors gained popularity in the 1990s as an alternative to CCP reactors [111]. As the processing requirements in the semiconductor industry became more stringent, the limitations of CCP reactors in independently controlling the plasma density (ion flux) and the ion bombardment energy motivated the search for alternative plasma sources. ICP sources provided a relatively simple transition. They operated at the same frequency as the conventional CCP reactors and their design was simpler than other alternative high-density sources such as electron cyclotron resonance microwave sources or helicon sources. ICPs typically achieve 10–100 times larger densities than CCP reactors while providing independent bias control.

ICPs use either a cylindrical or a planar coil to couple power to the plasma inductively. When an RF current is passed through the coil, a time-varying magnetic field is produced and, in turn, the time variation of the magnetic field induces an electric field that is parallel to the discharge chamber walls. This electric field accelerates the electrons and sustains the discharge. Since the electric field is parallel to the wall, the power is effectively coupled to the electrons in the discharge rather than to the ions in the sheath allowing higher plasma densities than CCP reactors [76, 77, 79, 80].

The power radiated from the coil of an ICP is absorbed in a small region of the plasma known as the skin layer. As for the CCP, it was experimentally observed that discharges could be maintained in an ICP reactor at low pressures where collisional heating is negligible [112]. Operation in this low-pressure regime is attributed to the anomalous skin effect [113, 114].

Despite all the advantages of ICPs over CCPs, the ICPs lack the uniformity of parallel plate reactors. As the semiconductor industry moves towards the use of larger wafers, uniformity becomes a very sensitive issue. In general, the uniformity of the discharge depends not only on the coil geometry but also on the pressure, gas composition, gas flow pattern and reactor size. As a result, several reactors and coil designs have been proposed over the years [115–117].

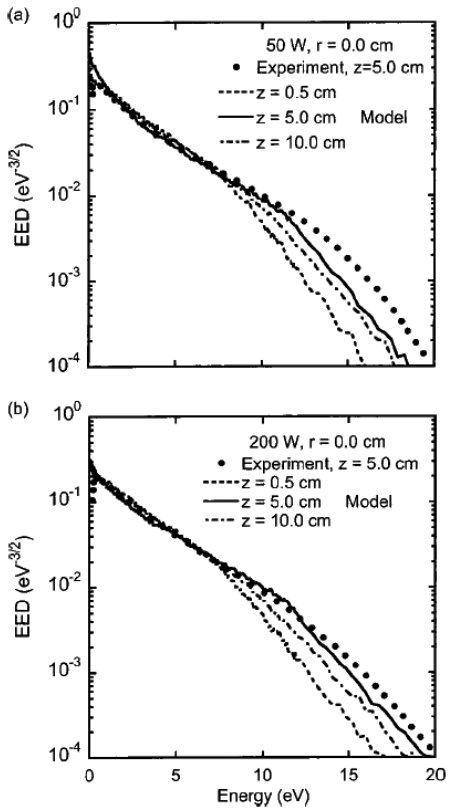

Figure 14. The EEDFs in the discharge centre, 6.78 MHz, 10 mTorr, for powers of: (*a*) 50 W and (*b*) 200 W. Simulation results are presented by lines while experimental data are given by symbols. Reprinted with permission from [118], copyright 2002 American Physical Society.

Simulation of low-pressure ICPs typically requires two- or three-dimensional models with detailed electron kinetic information. Multidimensional PIC simulations are computationally very intensive while fluid models cannot capture the non-local electron kinetics expected at low pressures. Hybrid models are therefore a natural choice for the simulation of these discharges.

5.1. Benchmark of hybrid simulations in ICPs: EEDFs

Figure 14 shows simulation results obtained by Vasenkov and Kushner [118] using a hybrid plasma equipment model and a comparison with experimental data. The model used in the simulation consists of three modules that are called iteratively until a converged solution is obtained. An electromagnetic module is used to calculate the fields, a particle module to determine electron-dependent properties and a fluid module to determine kinetics of heavy particles. In their work, the particle module incorporates not only elastic and inelastic collisions of electrons with heavy particles but also electron–electron Coulomb collisions. In ICPs where plasma density is sufficiently high, the electron–electron Coulomb collisions can play an important role, since the electron–electron collision frequency is proportional to the electron density. These are found to significantly affect the EEDF because the discharge has low-collisionality and presents a large degree of ionization. To capture the non-local behaviour of the electrons, the plasma

conductivity is calculated from the trajectories of electrons in the particle module instead of from the conventional local conductivity formula.

The simulations were performed on a 20 cm diameter planar ICP reactor operated in argon at 10 mTorr and excited at 6.78 MHz. The low-pressure of operation and the low excitation frequency favours the presence of non-local kinetics and the formation of an anomalous skin.

Good agreement can be observed between simulation and experimental results (figure 14). Although some discrepancies exist regarding the low-energy part of the EEDFs and the high-energy tail at low power levels, simulation results predict the general trend observed in experiments. At low power (50 W), the simulation results show the three-temperature Maxwellian distribution often encountered in low-pressure ICPs. As power increases to 200 W and higher density is obtained, the EEDF comes closer to a Maxwellian distribution. This change in EEDF is attributed to an increase in electron heating through electron–electron Coulomb collisions in the denser plasma. Although not shown here, good agreement was also observed by the axial variations of the effective electron temperature and electron density [118].

5.2. *Charged particle kinetics in ICPs*

As in the case of CCP reactors, the study of electron and ion kinetics in an ICP is very important as the transport of these particles determines the density and profiles of the discharge and thereby the process characteristics.

5.2.1. Ion kinetics: ion energy distribution function. In order to tailor the etching performance of an ICP discharge, it is desirable to be able to control the ion flux and the ion energy and angle distribution functions on the wafer independently. ICP reactors allow independent bias of the substrate and therefore permit better controllability than CCP reactors. The power delivered to the ICP antenna determines the plasma density, and thereby the ion flux, whereas the bias voltage applied to the wafer controls the ion energy. Although some coupling occurs between the bias power supply and the bulk plasma, this is significantly smaller than in a CCP reactor.

The mechanisms by which ions gain and exchange energy in the sheath region are similar to those in a CCP reactor. The IEDF on the wafer is determined by the ion transit time with respect to the excitation period and the collisionality within the sheath. As a result of the higher density typically encountered in ICPs, the sheath around the biased electrode is narrower in an ICP than in a CCP reactor. As a result, ions undergo typically fewer collisions.

When the ion transit time is much larger than the RF excitation period, ions respond to the average sheath potential, and in a collisionless case this leads to the formation of a single energy peak in the IEDF at the wafer. As the ion transit time becomes comparable to the RF excitation frequency, ions start responding to the instantaneous sheath voltage and the original single energy peak widens, forming two maxima. These maxima correspond to ions entering the sheath when the sheath voltage is at its maximum and minimum values. Since the ion transit time depends on the ion mass, different IEDFs should be expected for each species in the plasma.

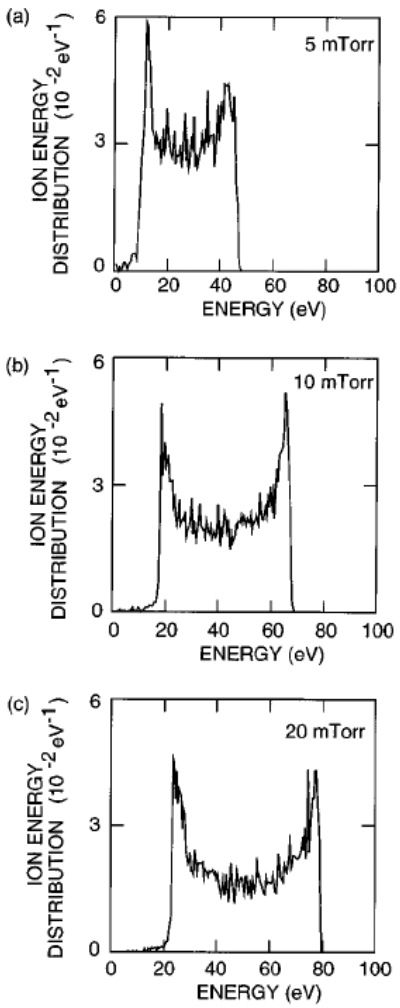

Figure 15. Simulation results of the ion energy distribution for Cl_2^+ for different pressures of: (*a*) 5 mTorr, (*b*) 10 mTorr and (*c*) 20 mTorr. Results were obtained for the RF bias of 100 V and ICP power of 500 W. Reprinted with permission from [119], copyright 1996 American Institute of Physics.

Figure 15 shows the IEDF of Cl_2^+ as a function of the gas pressure obtained in a hybrid simulation of an ICP reactor with an Ar/Cl_2 discharge [119]. Although the simulation incorporates a semi-analytical description of the sheath, it captures most of the physics one would expect. Unlike in the case of a CCP reactor at 67–100 mTorr (figure 12), the IEDFs in figure 15 present only two distinct maxima and do not extend from zero energy. When the pressure increases at a constant power, ion density increases and narrower sheaths are obtained for the same biased voltage. Since ions transit a narrower sheath in a shorter time, they become more sensitive to the instantaneous sheath voltage as the pressure increases and the IEDF widens (figure 15). The reduction of the sheath width also favours the collisionless character of the IEDF up to 20 mTorr for the power and bias conditions of the simulations. For the particular geometry studied in [119], an increase in pressure from 5 to 20 mTorr results in an increase of the dc bias potential on the wafer as indicated by the increasing average ion energy.

Although the IEDF is very important in determining process rates, the ion angle distribution function is equally

important in controlling the etching performance of the reactor. As the semiconductor industry moves towards nano-scale devices, etching of higher aspect ratio features is needed and more stringent constraints are put on the anisotropy of the process. Computer simulations incorporating plasma conditions and non-uniform charging of high-aspect ratio features can provide some insight into the ion kinetics and could lead to direct engineering solutions to this delicate issue.

5.2.2. Electron kinetics: anomalous skin effect. In an ICP discharge the power is delivered to the electrons in a thin layer near the antenna known as the skin layer. In the classical skin layer, electrons are heated through collisions and the electric field exponentially attenuates from the antenna into the plasma. The size of this layer depends on the plasma conductivity and typically it is of the order of 1–2 cm for an electron density of around 10^{11} cm^{-3}.

The operation of ICPs at low pressures where collisions are infrequent and ohmic heating is negligible, however, requires the heating of electrons in the skin layer by non-collisional means. When this occurs, the skin is anomalous [113, 114]. Collisionless electrons gain energy by entering the skin and returning to the bulk plasma upon reflection from the plasma sheath within a small fraction of the excitation period. This time-limited interaction with the high electric field present in the skin layer allows electrons to be accelerated and to retain the acquired energy by returning to the bulk plasma before the electric field reverses direction. Therefore, power can be deposited beyond the classical skin depth. This deeper penetration of the RF energy can be enhanced by the non-linear Lorentz force [120–122].

The non-linear interaction of hot electrons that have diffused back into the discharge with the local electric field can lead to the creation of regions of negative power deposition and non-monotonous electric field profiles. The regions of negative power deposition are created when electrons move with a phase difference larger than 90° with respect to the local electric field. Figure 16 shows the azimuthal electric field and the power deposition profile as a function of the distance from the antenna (height) at two different frequencies in a planar ICP reactor. The data were obtained using a hybrid plasma equipment model [118].

The electric field profile in the presence of an anomalous skin does not decay exponentially as in the case of a classical skin layer, and non-monotonic structures can appear. Regions of negative power deposition, however, can occur with monotonous and with non-monotonous fields (figure 16). The number of alternating positive and negative power deposition layers increases with frequency [118, 123].

The role of the magnetic field and the Lorentz force as well as resonances that can occur in a low-collisional discharge when the electron mean free path becomes comparable to the reactor size, have also been investigated [124–126]. The analysis of all these aspects taking into account the non-uniformity of the discharge is very complex, and computer simulations can provide some insight into the underlying physics of the discharge.

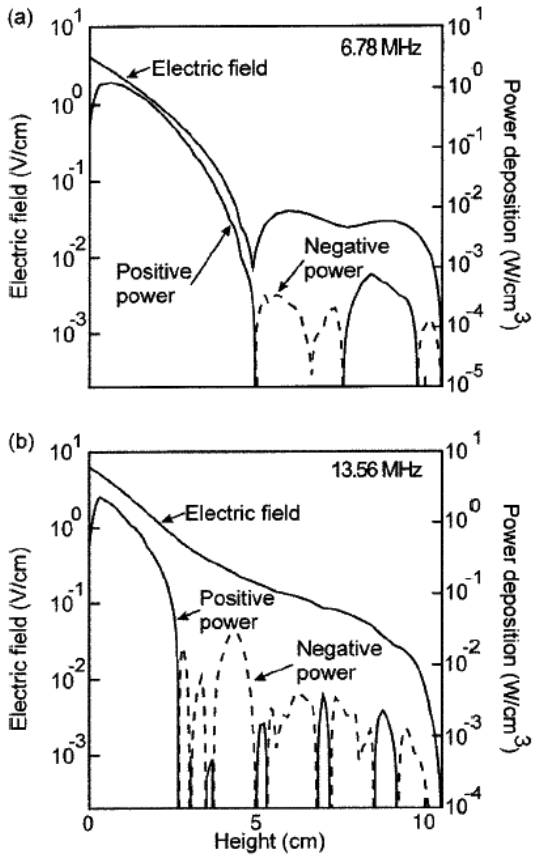

Figure 16. The θ component of the electric field and the power deposition in a 10 cm radius planar ICP at 100 W, 10 mTorr argon, $r = 4.5$ cm: (*a*) 6.78 MHz and (*b*) 13.56 MHz. Reprinted with permission from [118], copyright 2002 American Physical Society.

6. Conclusions

Modelling and computer simulation of low-temperature plasmas via particle, fluid and hybrid methods is spreading within the plasma community, both in academia and industry. This trend has been driven by the success of early works and the reduction in cost of computational resources. The usefulness of the simulation results, however, can be questioned if these do not agree with available experimental evidence. For that purpose, PIC, fluid and hybrid models were benchmarked by comparing simulation results and experimental data in the area of plasma displays, CCPs and ICPs. Excellent agreement can be found in these systems when the correct model is used for the simulation. Choosing the right model requires an understanding of the capabilities and limitations of the models and of the main physics governing a particular discharge. As simulation results continue to be validated by experiments, we can feel more confident in using computer simulations to improve our understanding of plasma physics as an alternative to analytical models and laboratory experiments. This can be particularly valuable in cases where analytical complexity or experimental difficulties prevent further analysis.

A brief overview of electron and ion kinetic effects in plasma displays, CCPs and ICPs was also presented. The capabilities of particle simulations to analyse kinetics problems are evident and particularly valuable when non-local

effects take place, and analytical complexity requires drastic assumptions.

Finally it should be mentioned that despite the achievements of modelling and computer simulation of low-temperature plasmas, particle, fluid and hybrid methods still need improvements in many aspects. Integration of different models with different spatial and time scales, speed-up techniques for long-duration, simulations and accurate fundamental parameters will further improve modelling and simulation results.

Acknowledgments

This work was supported in part by Lam Research Corporation, LG Electronics and the Korean Ministry of Science and Technology under the Teralevel Nano Devices Project, 21C Frontier R&D Program. Helpful comments from M J Kushner, F F Chen, C K Birdsall, J P Verboncoeur and H J Lee are gratefully acknowledged.

References

[1] Makabe T 2002 *Advances in Low Temperature RF Plasmas: Basis for Process Design* (Amsterdam: Elsevier)
[2] Birdsall C K and Langdon A B 1985 *Plasma Physics via Computer Simulation* (New York: McGraw-Hill)
[3] Tajima T 1988 *Computational Plasma Physics* (Redwood city: Addison-Wesley)
[4] Tien P K and Moshman J 1956 *J. Appl. Phys.* **27** 1067
[5] Buneman O 1959 *Phys. Rev.* **115** 503
[6] Birdsall C K and Bridges W B 1961 *J. Appl. Phys.* **32** 2611
[7] Dawson J M 1962 *Phys. Fluids* **2** 445
[8] Graves D B and Jensen K F 1986 *IEEE Trans. Plasma Sci.* **14** 92
[9] Graves D B 1987 *J. Appl. Phys.* **62** 88
[10] Park S K and Economou D J 1990 *J. Appl. Phys.* **68** 3904
[11] Makabe T and Nakano N 1992 *Phys. Rev.* A **45** 2520
[12] Ventzek P L G, Hoekstra R J and Kushner M J 1994 *J. Vac. Sci. Technol.* B **12** 461
[13] Deshmukh S and Economou D J 1993 *J. Vac. Sci. Technol.* B **11** 206
[14] Paranjpe A P 1994 *J. Vac. Sci. Technol.* A **12** 1221
[15] Kondo K, Kuroda H and Makabe T 1994 *Appl. Phys. Lett.* **65** 31
[16] Birdsall C K 1991 *IEEE Trans. Plasma Sci.* **19** 65
[17] Surendra M and Graves D B 1991 *IEEE Trans. Plasma Sci.* **19** 144
[18] Turner M M and Hopkins H B 1992 *Phys. Rev. Lett.* **69** 3511
[19] Verboncoeur J P, Alves M V, Vahedi V and Birdsall C K 1993 *J. Comput. Phys.* **104** 321
[20] Vahedi V and Surendra M 1995 *Comput. Phys. Commun.* **87** 179
[21] Boeuf J P 1987 *Phys. Rev.* A **36** 2782
[22] Kinder R L, Ellingboe A R and Kushner M J 2003 *Plasma Sources Sci. Technol.* **12** 561
[23] Gogolides E and Sawin H H 1992 *J. Appl. Phys.* **72** 3971
[24] Kim H C, Yang S S and Lee J K 2003 *J. Appl. Phys.* **93** 9516
[25] Sadiku M 2001 *Numerical Techniques in Electromagnetics* (Boca Raton, FL: CRC Press)
[26] Scharfetter D and Gummel H 1969 *IEEE Trans. Electron Devices* **16** 64
[27] Selberherr S 1984 *Analysis and Simulation of Semiconductor Devices* (Wien: Springer)
[28] Passchier J D P and Goedheer W J 1993 *J. Appl. Phys.* **74** 3744
[29] Kushner M J 2004 *J. Appl. Phys.* **95** 846
[30] Iza F, Yang S S, Kim H C and Lee J K 2005 *J. Appl. Phys.* at press
[31] Hockney R W and Eastwood J W 1981 *Computer Simulation Using Particles* (New York: McGraw-Hill)
[32] Verboncoeur J P 2005 *Plasma Phys. Control. Fusion* **47** A231
[33] Langdon A B 1970 *J. Comput. Phys.* **6** 247
[34] Langdon A B and Birdsall C K 1970 *Phys. Fluids* **13** 2115
[35] Okuda H 1972 *J. Comput. Phys.* **10** 475
[36] Chen L, Langdon A B and Birdsall C K 1974 *J. Comput. Phys.* **14** 200
[37] Skullerud H R 1968 *Br. J. Appl. Phys.* **1** 1567
[38] Kawamura E, Birdsall C K and Vahedi V 2000 *Plasma Sources Sci. Technol.* **9** 413
[39] Hitchon W N G 1999 *Plasma Processes for Semiconductor Fabrication* (Cambridge: Cambridge University Press) p 161
[40] Vahedi V, DiPeso G, Birdsall C K, Lieberman M A and Rognlien T D 1993 *Plasma Sources Sci. Technol.* **2** 261
[41] Manuilenko O 2004 private communication
[42] Meyer P and Wunner G 1997 *Phys. Plasmas* **4** 3152
[43] Shon C H, Lee H J and Lee J K 2001 *Comput. Phys. Commun.* **141** 322
[44] Sommerer T J and Kushner M J 1992 *J. Appl. Phys.* **71** 1654
[45] Lee J K and Birdsall C K 1979 *Phys. Fluids* **22** 1315
[46] Porteous R K and Graves D B 1991 *IEEE Trans. Plasma Sci.* **19** 204
[47] Lee J K and Verboncoeur J P 2001 *Low Temperature Plasma Physics* ed R Hippler *et al* (Berlin: Wiley-VCH) p 367
[48] Boeuf J P 2003 *J. Phys. D: Appl. Phys.* **36** R53
[49] Rauf S and Kushner M J 1999 *J. Appl. Phys.* **85** 3460
[50] Punset C, Cany S and Boeuf J P 1999 *J. Appl. Phys.* **86** 124
[51] Shin Y K, Shon C H, Kim W and Lee J K 1999 *IEEE Trans. Plasma Sci.* **27** 1366
[52] Yang S S, Kim H C, Ko S W and Lee J K 2003 *IEEE Trans. Plasma Sci.* **31** 596
[53] Lee H J, Kim H C, Yang S S and Lee J K 2002 *Phys. Plasmas* **9** 2822
[54] Kim H C, Hur M S, Yang S S, Shin S W and Lee J K 2002 *J. Appl. Phys.* **91** 9513
[55] Kim H C, Yang S S and Lee J K 2002 *IEEE Trans. Plasma Sci.* **30** 188
[56] Yang S S, Lee J K, Ko S W, Kim H C and Shon J W 2004 *Contrib. Plasma Phys.* **44** 536
[57] Drallos P J, Nagorny V P and Williamson W Jr 1995 *Plasma Sources Sci. Technol.* **4** 576
[58] Shin Y K, Lee J K, Shon C H and Kim W 1999 *Japan. J. Appl. Phys.* **38** L174
[59] Fridman A, Chirokov A and Gutsol A 2005 *J. Phys. D: Appl. Phys.* **38** R1
[60] Tachibana K, Mizokami K, Kosugi N and Sakai T 2003 *IEEE Trans. Plasma Sci.* **31** 68
[61] Shintani Y, Ahn J C, Tachibana K, Sakai T and Kosugi N 2003 *J. Phys. D: Appl. Phys.* **36** 2928
[62] Yang S S, Ko S W, Kim H C, Mukherjee S and Lee J K 2003 *Proc. Int. Meeting on Information Display (Daegu, Korea)* p 739
[63] Motoyama Y, Matsuzaki H and Murakami H 2001 *IEEE Trans. Electron Devices* **48** 1568
[64] Choi E H, Lim J Y, Kim Y G, Ko J J, Kim D I, Lee C W and Cho G S 1999 *J. Appl. Phys.* **86** 6525
[65] Piscitelli D, Pitchford L C and Boeuf J P 2000 *Proc. Int. Display Workshps (Kobe, Japan)* p 735
[66] Hagelaar G J M and Kroesen G M W 2000 *J. Appl. Phys.* **88** 2240
[67] Yang S S, Kim S J and Lee J K 2004 *J. Plasma Fusion Res.* **80** 132
[68] Yang S S, Ko S W, Mukherjee S and Lee J K 2003 *Proc. Int. Display Workshops (Fukuoka, Japan)* p 885
[69] Verboncoeur J P, Langdon A B and Gladd N T 1995 *Comput. Phys. Commun.* **87** 199
[70] Park W B, Lim J Y, Oh J S, Jeong H S, Cho G S and Choi E H 2003 *Int. Display Workshops (Fukuoka, Japan)* p 973
[71] Cho G, Choi E H, Kim Y G, Kim D I, Uhm H S, Joo Y D, Han J G and Kim M C 2000 *J. Appl. Phys.* **87** 4113

[72] Callegari Th, Ganter R, Guillot Ph, Galy J and Boeuf J P 1999 *Proc. Int. Display Workshops (Sendai, Japan)* p 663
[73] Shon C H and Lee J K 2001 *Phys. Plasmas* **8** 1070
[74] Lee J K, Dastgeer S, Shon C H, Hur M S, Kim H C and Cho S W 2001 *Japan. J. Appl. Phys.* **40** 528
[75] Kolobov V I and Godyak V A 1995 *IEEE Trans. Plasma Sci.* **23** 503
[76] Lieberman M A and Lichtenberg A J 1994 *Principles of Plasma Discharges and Materials Processing* (New York: Wiley)
[77] Chen F F and Chang J P 2003 *Lecture Notes on Principles of Plasma Processing* (New York: Kluwer/Plenum)
[78] Raizer Yu P, Shneider M N and Yatsenko N A 1995 *Radio-Frequency Capacitive Discharges* (Boca Raton: CRC Press)
[79] Roth J R 2001 *Industrial Plasma Engineering Vol. 2: Applications to Nonthermal Plasma Processing* (Bristol: Institute of Physics Publishing)
[80] Fridman A and Kennedy L A 2004 *Plasma Physics and Engineering* (New York: Taylor and Francis)
[81] Surendra M and Graves D B 1991 *Appl. Phys. Lett.* **59** 2091
[82] Goto H H, Lowe H D and Ohmi T 1992 *J. Vac. Sci. Technol.* A **10** 3048
[83] Kitajima T, Takeo Y and Makabe T 1999 *J. Vac. Sci. Technol.* A **17** 2510
[84] Robiche J, Boyle P C, Turner M M and Ellingboe A R 2003 *J. Phys. D: Appl. Phys.* **36** 1810
[85] Kim H C, Lee J K and Shon J W 2003 *Phys. Plasmas* **10** 4545
[86] Kim H C and Lee J K 2005 *J. Vac. Sci. Technol.* A **23** 651
[87] Kim H C and Lee J K 2004 *Phys. Rev. Lett.* **93** 085003
[88] Kim H C and Lee J K 2005 *Phys. Plasmas* **12** 053501
[89] Godyak V A and Piejak R B 1990 *Phys. Rev. Lett.* **65** 996
[90] Kaganovich I D 2002 *Phys. Rev. Lett.* **89** 265006
[91] Kim H C, Park G Y and Lee J K 2005 submitted
[92] Radmilović-Radjenović M and Lee J K 2005 *Phys. Plasmas* **12** 063501
[93] Shon J W 2004 private communication
[94] Kropotov N Yu, Kachanov Yu A, Reuka A G, Lisovskiy V A, Erorenkov V D and Farenik V 1988 *Sov. Tech. Phys. Lett.* **14** 159
[95] Lisovskiy V A and Yegorenkov V D 1994 *J. Phys. D: Appl. Phys.* **27** 2340
[96] Radmilović-Radjenović M, Lee J K, Iza F and Park G Y 2005 *J. Phys. D: Appl. Phys.* **38** 950
[97] Vaughan J R M 1989 *IEEE Trans. Electron Devices* **36** 1963
[98] Vaughan J R M 1993 *IEEE Trans. Electron Devices* **40** 830
[99] Phelps A V and Petrović Z Lj 1999 *Plasma Sources Sci. Technol.* **8** R21
[100] Phelps A V, Pitchford L C, Pedoussat C and Donko Z 1999 *Plasma Sources Sci. Technol.* **8** B1
[101] Theiberger P, Hanson A L, Steski D B, Zajic V, Zhang S Y and Ludewig H 2000 *Phys. Rev.* A **61** 042901
[102] Thomas E W 1984 *Nucl. Fusion* **94** 94
[103] Kim H C, Manuilenko O and Lee J K 2005 *Japan. J. Appl. Phys.* **44** 1957
[104] Vahedi V, DiPeso G, Birdsall C K, Lieberman M A and Rognlien T D 1993 *Plasma Sources Sci. Technol.* **2** 273
[105] Schweigert I V and Schweigert V A 2004 *Plasma Sources Sci. Technol.* **13** 315
[106] Kawamura E, Vahedi V, Lieberman M A and Birdsall C K 1999 *Plasma Sources Sci. Technol.* **8** R45
[107] Babaeva N Yu, Shon J W, Hudson E A and Lee J K 2005 *J. Vac. Sci. Technol.* A **24** 699
[108] Lee J K, Manuilenko O V, Babaeva N Yu, Kim H C and Shon J W 2005 *Plasma Sources Sci. Technol.* **14** 89
[109] Wild C and Koidl P 1991 *J. Appl. Phys.* **69** 2909
[110] Godyak V A, Piejak R B and Alexandrovich B M 1992 *Phys. Rev. Lett.* **68** 40
[111] Hopwood J 1992 *Plasma Sources Sci. Technol.* **1** 109
[112] Hopwood J, Guarnieri C R, Whitehair S J and Cuomo J J 1993 *J. Vac. Sci. Technol.* A **11** 152
[113] Turner M M 1993 *Phys. Rev. Lett.* **71** 1844
[114] Kolobov V I and Economou D J 1997 *Plasma Sources Sci. Technol.* **6** R1
[115] Wu X and Lieberman M A 2000 *Plasma Sources Sci. Technol.* **9** 210
[116] Kim S S, Chang H Y and Chang C S 2000 *Appl. Phys. Lett.* **77** 492
[117] Meziani T, Colpo P and Rossi F 2001 *Plasma Sources Sci. Technol.* **10** 276
[118] Vasenkov A V and Kushner M J 2002 *Phys. Rev.* E **66** 066411
[119] Hoekstra R J and Kushner M J 1996 *J. Appl. Phys.* **79** 2275
[120] Evans J D and Chen F F 2001 *Phys. Rev. Lett.* **86** 5502
[121] Cohen R H and Rognlien T D 1996 *Plasma Sources Sci. Technol.* **5** 442
[122] Godyak V A, Piejak R B and Alexandrovich B M 1999 *Phys. Rev. Lett.* **83** 1610
[123] Godyak V A and Kolobov V I 1997 *Phys. Rev. Lett.* **79** 4589
[124] Rauf S and Kushner M 1997 *Plasma Sources Sci. Technol.* **6** 518
[125] Tyshetskiy Yu O, Simolyakov A I and Godyak V A 2002 *Plasma Sources Sci. Technol.* **11** 203
[126] Godyak V A and Kolobov V I 1997 *Phys. Rev. Lett.* **81** 369